Contents lists available at SCCE

Journal of Soft Computing in Civil Engineering

Journal homepage: www.jsoftcivil.com

Hybrid Models for Basalt Building Stones Assessment: Combining Regression and LSTM Techniques

Samer Rababah [1,*]; Mohammad Ali Khasawneh [2]; Hiren Mewada [3]; Hussien Aldeeky[4]

1. Dept. of Civil Engineering, Jordan University of Science &Technology, P.O. Box 3030, Irbid 2210, Jordan
2. Civil Engineering Department, Prince Mohammad Bin Fahd University, P.O. Box 1664, 31952 Al Khobar, Kingdom of Saudi Arabia
3. Electrical Engineering Department, Prince Mohammad Bin Fahd University, P.O. Box 1664, 31952 Al Khobar, Kingdom of Saudi Arabia
4. Department of Civil Engineering, Faculty of Engineering, The Hashemite University, P.O. Box 330127, Zarqa 13133, Jordan

* Corresponding author: *srrababah@just.edu.jo*

https://doi.org/10.22115/scce.2025.2017

ARTICLE INFO

Article history:
Received: 16 January 2025
Revised: 09 July 2025
Accepted: 07 August 2025

Keywords:
Uniaxial compressive strength;
Tangent modulus of elasticity;
Long short term memory (LSTM);
Leeb rebound hardness;
Schmidt hammer;
Dry density;
Ultrasonic pulse velocity.

ABSTRACT

Because basalt rock is durable, abundant, hard and visually appealing, it has been widely used in the construction of many historical buildings in Jordan. Over time, these structures quite often require routine maintenance to preserve their structural integrity. Key parameters for assessing its mechanical behavior are uniaxial compressive strength (UCS) and the tangent modulus of elasticity (Et). However, direct laboratory tests to measure both UCS and Et require a specific core sample with certain dimensions, which is expensive, time-consuming, and prohibited in historic buildings. For this reason, developing novel models to predict both UCS and Et of basalt rock based on simple nondestructive tests is required. A laboratory of 134 datasets has been tested and used as input data, including Leeb rebound hardness (LRH), Schmidt hammer (Rn), Dry Density (DD), and ultrasonic pulse velocity (UPV). The study compares three approaches: simple regression models, multiple linear regression (MLR), and nonlinear regression (NLR), alongside advanced machine learning models, such as Long Short-Term Memory (LSTM) networks. A low Durbin-Watson (DW) value indicated significant positive autocorrelation in the residuals, suggesting temporal or sequential dependency in the data. This finding makes LSTM networks particularly well suited for modeling UCS and Et. Results show that although MLR and NLR are effective in prediction, LSTM models outperform them in accuracy, with R2 values of 0.9815 and 0.9644 for predicting UCS and Et, respectively, and lower RMSE values of 5.3135 and 0.7229 for predicting UCS and Et, respectively. The findings demonstrate the potential of combining traditional statistical methods with advanced machine learning approaches to estimate the mechanical properties of basalt rock accurately.

How to cite this article: Rababah S, Khasawneh M, Mewada H, aldeeky H. Hybrid models for basalt building stones assessment: combining regression and LSTM techniques. Journal of Soft Computing in Civil Engineering. (2026);10(2): 2017. https://doi.org/10.22115/scce.2025.2017

1. Introduction

Basalt rocks were used in ancient architecture at various archaeological sites in Jordan throughout history, particularly in areas where the material was locally available. Due to its unique properties, such as being extremely hard, stable, and adaptable to most climates, it was widely used as a building material. These heritage buildings possess high cultural, historical, and architectural value, and it is essential to preserve them. As a result, their mechanical characteristics and load-bearing capacity can only be assessed using very limited testing techniques due to their heritage status, unique materials, and fragile condition.

Uniaxial compressive strength (UCS) and tangent modulus of elasticity (Et) are categorized as the key factors that define the rock's mechanical behavior [1]. These parameters are utilized in numerical modeling, material classification, construction, and design optimization. The International Society for Rock Mechanics [2] requires a specific core sample with certain dimensions, which is expensive and time-consuming [3–5]. However, sampling such materials is rather problematic and may require considerable time and effort, particularly in the case of soft, weathered, fractured, and foliated rocks. On the other hand, preservation concerns often prevent sampling of heritage or historical buildings and facilities. Due to its being invasive and destructive, uniaxial compression testing is not practical for use in such situations. For this reason, alternative methods for determining UCS without sacrificing structural or material integrity are necessary.

To mitigate the shortcomings of traditional UCS testing, researchers have developed various portable and effective index testing techniques that serve as reliable substitutes. By correlating UCS with easier, non-invasive measurements through empirical models, these methods allow efficient strength evaluation without the need for destructive procedures. These techniques include porosity analysis, dry density calculation, point load testing, ultrasonic pulse velocity measurement and Schmidt hammer rebound testing. Other approaches include Brinell hardness measurements, Shore scleroscope hardness evaluations, Leeb rebound hardness tests, and slake durability assessments, which have all been used to estimate UCS and the tangent modulus of elasticity with varying degrees of accuracy [6,7]. These methods offer useful alternatives to rock strength determination when conventional UCS testing is not feasible or practical.

Recently, simple regression, multivariable regression, various types of machine learning, and soft computing have been employed to predict UCS and Et from simple laboratory tests [8]. However, predictive modeling was only possible until recently to analyze simple linear relationships between datasets. The advance of deep learning techniques makes it possible to predict complex, nonlinear relationships through the use of large datasets. For this domain, the very high effectiveness of deep networks in learning complex data patterns has resulted in massive improvements in prediction accuracy. Recently, many researchers have applied machine learning methods to predict UCS and Et, showing that these advanced methods can be used for material property estimation [9–13].

Ghasemi et al. (2018) utilized the trees model to estimate UCS and Et based on simple indices, including ultrasonic pulse velocity, effective porosity, dry unit weight, Schmidt hardness, and slake durability [14]. In the work of Mahmoodzadeh et al. (2022), rock strength parameters were predicted using KNN (K nearest neighbor), SVR (support vector regression), GPR (Gaussian process regression) and DT (decision tree) approaches [15].

The results showed that GPR is the most suitable method for predicting the UCS of sedimentary rock. In their study of weak rock, Shahani et al. (2022) employed artificial neural networks (ANN), Adaptive Neuro-Fuzzy Inference Systems (ANFIS), and Multivariate linear regression (MVLR) methods for estimating USC and found that ANFIS is the most effective method for predicting USC [9]. The result of Sabri et al.

(2024) using SVR, ANN, and ANN-PSO (particle swarm optimization) was that the ANN-PSO method can predict the UCS value with 80% accuracy [16]. The result of Wen et al. (2024) was further utilized in an ANN and PSO least squares support vector regression (LSSVR) model to predict the USC value. By using their result, they found that the hybrid PSO-LSSVR method is suitable for estimating the UCS value with 98% accuracy. Table 1 summarizes some previous studies on various predictive models [17].

Table 1
Summary of previous studies on various predictive models.

References	Model type	Model input	Model output
[18]	GEP, ANN	n, R_n, V_p, ρ_d, w_a	UCS, σ_t
[19]	SR, MLR	UCS, ρ, σ_t	BI_m
[20]	SR, ANN	n, $Is_{(50)}$, R_n, V_p	UCS, Et
[21]	PSO	UCS, BTS, BI, DPW, Alpha Angle	ROP
[22]	SR, NMR, ANN	n, R_n, ρ_d, V_p, ρ_s, ρ_b, I_d	UCS, Et
[23]	SR, MLR, GEP	n, ρ, V_p	UCS, Et
[24]	SR, MLR, ANN, ANFIS	V_p, BPI, $Is_{(50)}$, σ_t	UCS
[25]	MLR, ANN, ICA-ANN	n, V_p, $Is_{(50)}$	UCS, Et
[26]	ANN	ρ, $Is_{(50)}$,V_p, σ_t	UCS
[5]	ANFIS	n, ρ, V_p	UCS, Et
[27]	ANN, ANFIS, SVM	cell pressure, strain rate, temperature, time, strain	σ_{tc}, E
[28]	MLR, NMR, ANN, ANFIS.	$Is_{(50)}$, BPI, and cylinder punch tests.	UCS, Et
[11]	ANN, MLR	ρ_d, V_p, $Is_{(50)}$, R_n, σ_t, I_d	UCS
[29]	SR, MLR, ANN, ANFIS, and GEP	γ, $Is_{(50)}$, σ_t, SH, R_n, V_p	UCS
[30]	ANN, ICA–ANN, ABC–ANN, GP	n, $Is_{(50)}$, R_n	UCS
[31]	MLPNN, M5MT, ELM	σ_t, V_p, SH, $Is_{(50)}$	UCS
[32]	GPR, DT, SVR, LSTM, DNN, KNN,	V_p, SH, n, $Is_{(50)}$	UCS
[33]	a hybrid GWO-ELM	V_p, SH, n, $Is_{(50)}$	UCS, Et
[10]	MLR, M5MT, KNN, ANN, SR and MLR	ρ_d, V_p, $Is_{(50)}$, R_n, n	UCS
[34]	RF, AdaBoost, CatBoost, XGBoost	n, ρd , Vp, I_d , w_a	UCS, Et
[35]	AR, bagging, M5, M5P, RF, SVR, LWL, GPR, MLP	cell pressure, strain rate, temperature, time, strain	E
[36]	ANN	Section Images	UCS, Et

$Is_{(50)}$: point load strength index, R_n: Schmidt hammer rebound number, V_P: P-wave velocity, n: porosity, ρ: density, w_a: water absorption, σ_t: brazilian tensile strength, BI_m: brittleness index, γ: Unit Weight, ρ_d: dry density, ρ_s: saturated density, ρ_b: buoyant density, DPW: distance between the planes of weakness, ROP: TBM rate of penetration, BPI: Block Punch Index, w: water content, SH: shore hardness, I_d: Slake Durability Index, σtc = triaxial compressive strength; E = Young's modulus;

GEP: Gene expression programming, SR: Simple regression, MLR: multiple regression analysis, NMR: nonlinear multiple regression, MLPNN: Multilayer Perceptron Neural Network, PSO: Particle Swarm Optimization, ANFIS: Adaptive neuro-fuzzy inference system, GP: genetic programming, ELM: Extreme Learning Machine, M5MT: M5 Model Tree, GWO-ELM: Extreme Learning Machine with Gray Wolf Optimization, SVR: support vector regression, ICA: Imperialist competitive algorithm, ABC: artificial bee colony. RF: random forest, AR: additive regression, LWL: locally weighted linear, GPR: Gaussian process regression, MLP: multi-layered perceptron neural network.

Long Short-Term Memory (LSTM) is the best architecture among all deep learning architectures for learning from sequential data and capturing temporal dependencies and complex patterns in the dataset [37,38]. It differs from feed-forward neural structures, and its purpose is to preserve input information for longer time frames, which makes LSTMs very useful for time series data and sequential inputs. This capability enables LSTMs to capture temporal dependencies and trends that might exist between the input features.

Therefore, their use in predicting mechanical properties that may be affected by historical data patterns is not only logical but also beneficial. In this study, a set of predetermined input parameters is used to predict UCS and Et with Long LSTM networks. LSTMs are a refined form of recurrent neural network (RNN) designed to process sequential data by retaining information for lengthy periods.

In this study, various predictive methods, including simple regression, multiple linear regression (MLR), nonlinear regression (NLR), and LSTM networks, are employed to predict the mechanical properties of the UCS of basalt rocks. The predictions are based on cost-effective nondestructive techniques that utilize the rock's physical and mechanical properties, such as dry density, pulse velocity, Schmidt hammer rebound and Leeb rebound hardness.

2. Materials and methods

2.1. Material

Basalt rock is commonly used in construction due to its widespread availability in Jordan (Fig. 1), where it occupies an area of approximately 11,400 km², accounting for 11% of the country's total area [6]. The basalt used in construction was derived from volcanic activity in the late Cenozoic era, which was common across Jordan. Notably, the Harrat Ash Shaam region in northern and eastern Jordan has abundant basalt deposits.

Different Jordanian archaeological sites show evidence of basalt's use in ancient architecture (Fig. 2). Environmental factors, such as heat and the arid climate, did not have a negative impact on these ancient buildings over the millennia because basalt is naturally resistant to such adverse conditions. A good example is the city of Umm al-Jimal (in the east Jordan desert), where basalt was used in the construction of pathways, walls and columns.

Similarly, basalt is incorporated in many structural elements in Umm Qais (Gadara) to show the importance of basalt in the construction of both civic and religious buildings. It was ideal for making defensive structures and would ensure the longevity of the city walls and other fortifications. The basalt’s aesthetic appeal was another factor that contributed to its high popularity among architects and builders. When used in conjunction with lighter stones, such as limestone, it was often employed in the design of buildings, as evident in ancient Jordan.

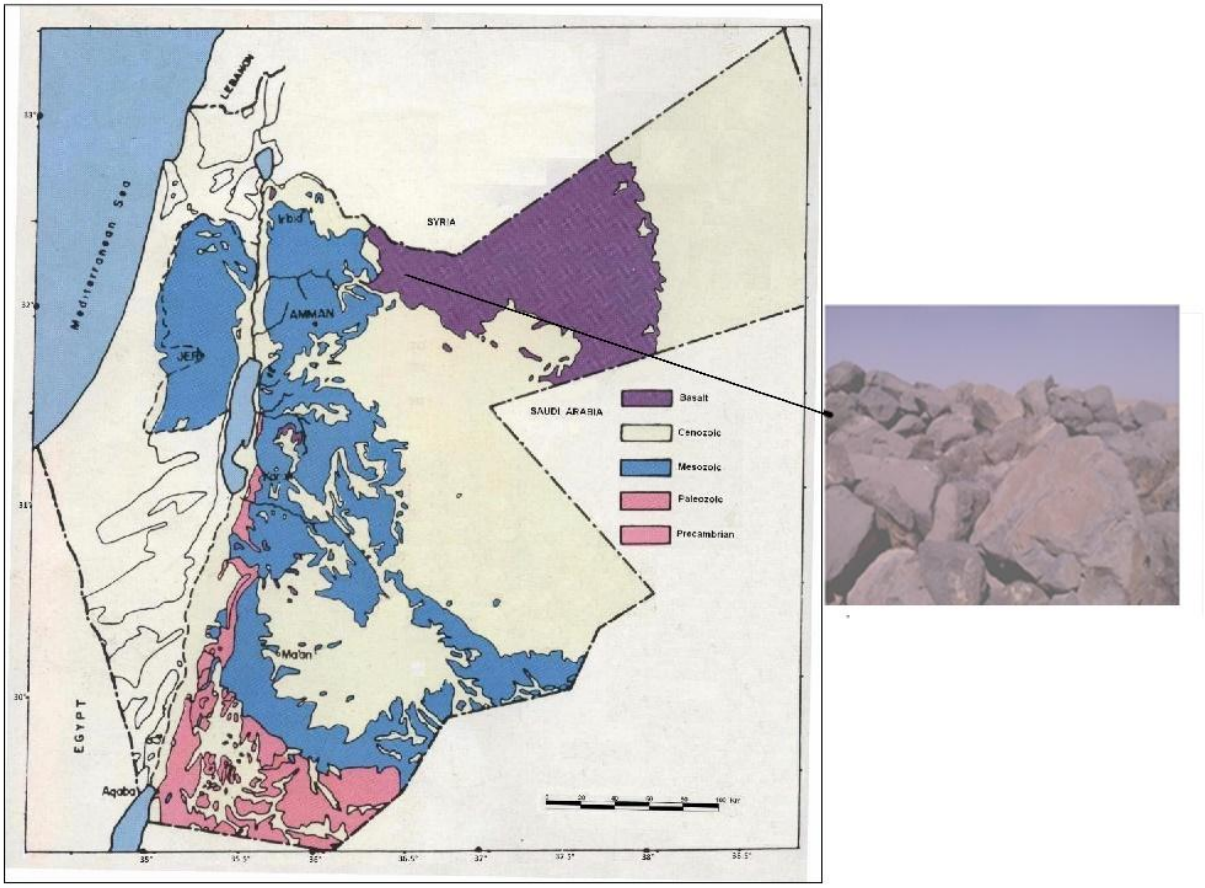

Fig. 1. Distribution of basalt rock in Jordan.

Fig. 2. Images showcasing historic basalt buildings and cities in Jordan (a) Qasr Al-Azraq, (b) Um-Qais, (c) Qasr Al Hallabat and Qastal, and (d)Um-Al Jimal.

2.2. Sample and test method

X-ray Fluorescence Spectrometry (XRF) was used to determine the major and minor oxide contents of the rock samples (Table 2). The basalt rock in this study is classified as a mafic alkaline basalt.

Table 2
XRF analysis of the studied basalt samples.

Oxides	Average Percentage, %
SiO_2	45.1
Fe_2O_3	14.3
Al_2O_3	12.4
CaO	11.5
MgO	8.4
TiO_2	1.7
Na_2O	3.4
K_2O	0.7
P_2O_5	0.3
MnO	0.2
L.O.I	2.1

An X-ray diffractometer (XRD) was used for mineralogical work. For this test, a randomly oriented powder mount method was used. Before testing, the rock samples were first crushed and ground to a particle size of 0.040 mm (325 mesh). Approximately 1 g of the fine powder sample was placed on the sample holder for X-ray diffraction analysis. The samples were qualitatively scanned at a 2-theta angle of 5° to 65° using Cu Kα radiation and a scanning speed of 2° per minute to obtain precise diffraction data. The XRD test results showed that the major minerals identified in the samples under consideration are plagioclase, pyroxene, magnetite and olivine. These minerals are typical of basaltic rock compositions. The detailed diffraction patterns supporting these findings are presented in Fig. 3.

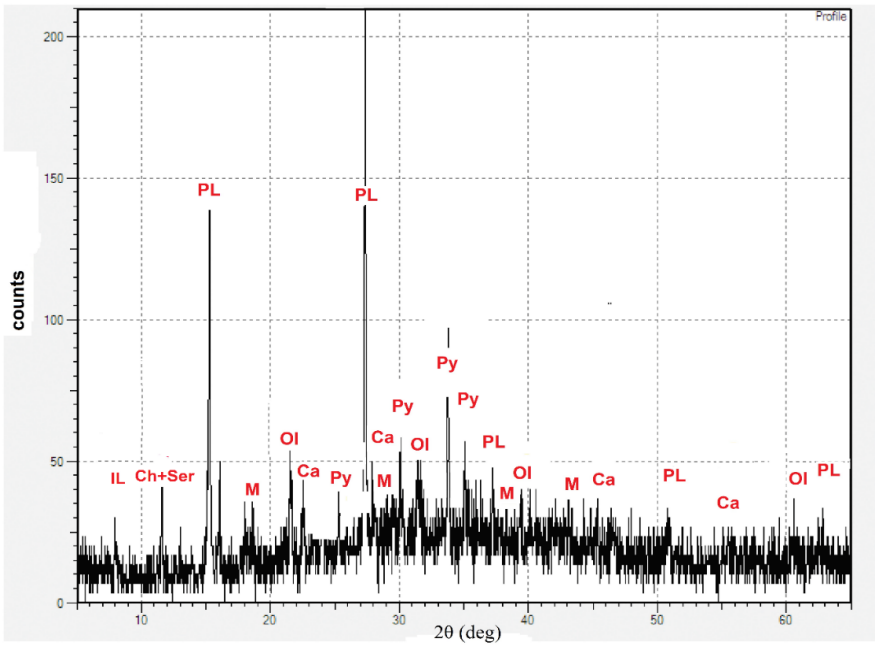

Fig. 3. XRD analysis of studied basalt samples (PL: plagioclase, Py: pyroxene, O: olivine, M: magnetite, C: calcite, Ch: Chlorite, Ser: Sericite).

Leeb rebound hardness (LRH), Schmidt hammer(Rn), dry density(DD), ultrasonic pulse velocity (UPV), Uniaxial compressive strength (UCS), and tangent modules of elasticity (Et) were conducted. 134 NX cylindrical core samples with a diameter of 64.0 mm and length of 13.0-15.0 cm were taken from different boulders throughout the study area; these core samples were prepared to reach a ratio of length/diameter 2:1 and polished to reach a smooth surface according to ASTM D4543 (2008) and [39].

Before the lab testing, all prepared samples were marked and labeled, and the specimen geometry was verified to minimize errors during the experiments. The volume of the specimen was determined by measuring its diameter and length with a caliper to obtain the appropriate values. After that, to remove any moisture content from the specimen, it was left in the oven at 105°C for 24 hours before being subjected to further tests.

The UPV test is a simple, non-destructive test that determines the quality of natural rocks by measuring wave transmission through the specimen and the propagation time. High pulse velocities indicate good quality and continuity because waves encounter little resistance as they pass through solid, dense material. Rock strength may be indicated by slower pulse velocities. The PUNDIT Pulse (Portable Ultrasonic Nondestructive Digital Indicating Tester), as used by [39] and [40] on cylindrical rock core specimens with a diameter of 64 mm and a frequency of 54 kHz, was employed. The ultrasonic pulse transit time through the core sample was measured, and the ultrasonic pulse velocity was calculated by dividing the core sample length by the measured ultrasonic pulse transit time.

For this study, the LRH test was chosen because, compared to most testing methods, it is minimally invasive and can accurately measure thin layers. Additionally, LRHT is highly efficient because tests can be conducted within a few seconds. The main benefit of this device is that it is capable of measuring both soft and thin materials, as it utilizes low-impact energy that does not harm the material's surface. Because there is no standard for carrying LRH on rock samples, the test procedure was modified based on the guidelines provided by [41,42]. Repeating their methodology, the single-impact method was employed; therefore, each core specimen received 12 impacts. To minimize error, the highest and lowest values were omitted, and the average of the remaining ten values was used to measure hardness.

The R_n test is the most frequently applied method for determining the relative intensity of rock strength, which estimates the hardness of the rock at its exposed surface without destroying it. This non-destructive method is fast, easy to perform, and inexpensive; therefore, it can be conducted in either the field or the laboratory. They are useful for a preliminary indication of the strength and quality of rock mass materials. In this study, a total of 134 core samples with a 64mm diameter were tested using an L-type Schmidt hammer device, following the procedure according to [43]. First, the rock sample was fixed, and the hammer was held vertically downward at a right angle. Moreover, a total of 20 readings were recorded at different locations, and the average of the ten highest values was used in this study as an R_n.

The UCS and Et tests were performed according to the [44] standards using a computerized compression testing machine with a maximum load of 2000 kN. Under a constant stress rate of 5 MPa/s, the tests were conducted to maintain consistent loading conditions throughout the process. The maximum ultimate stress that the rock specimen could withstand under uniaxial loading before failure was defined as the UCS value. The stress-strain behavior of the rock sample was analyzed to calculate the Et. Et was taken as the slope of the stress-strain curve at a point representing 50% of the UCS value [45,46].

2.3. Regression analysis

Researchers commonly use simple regression (SR) methods to develop predictive correlations between the mechanical properties of rocks, particularly UCS and Et, and parameters obtained in nondestructive testing methods. Usually, parameters such as ultrasonic pulse velocity, dry density, and rebound hardness are considered because they can be measured quickly with no damage created to the rock samples. These correlations have been continuously predicted using regression models, which enable fast and low-cost estimations of rock strength; many studies have already proven their reliability [3,4,11,47].

Multiple Linear Regression (MLR) is a technique used to analyze and predict dependent variables in terms of several independent variables. Simple regression is the study of the effect on an outcome of a single dependent and a single independent variable, whereas MLR considers two or more predictors that would predictively affect a dependent variable outcome. It ascertains which predictors will prove most beneficial to the outcome and the form in which these predictors interact with each other. MLR evaluates variability by determining how much of the change in the dependent variable is explained by the independent variables in the model. The data must satisfy certain assumptions, including linearity and the absence of multicollinearity among predictors. Predictors could be highly correlated with one another, which, in turn, can lead to the inflation of standard errors and compromise the statistical significance of coefficients when conducting analysis.

Additionally, the data must satisfy certain assumptions, such as linearity and the absence of multicollinearity among predictors. When there are highly correlated predictors, this can lead to inflated standard errors and undermine the statistical significance of coefficients when conducting an analysis. Multicollinearity occurs when predictors are highly correlated, potentially inflating standard errors and compromising the statistical significance of coefficients.

Nonlinear regression (NLR) is a technique used to describe the connections between a dependent variable and one or more specified independent variables, where these connections exhibit nonlinearity. In nonlinear regression, the relation between the variables can be captured in a nonlinear equation or as a curve. Nonlinear regression can represent complex behaviors, such as exponential growth, log trends, and sinusoidal behavior, that straight-line models cannot predict. To minimize the difference between observed and predicted values, different techniques, such as least squares, were often used to estimate model parameters. However, the NLR has its drawbacks, which include sensitivity to initial parameter estimates, an overfitting risk, and model choice sensitivity. Also, linear regression is more computationally intensive than this one. NLR is nevertheless a powerful analytical tool that can approximate extremely nonlinear relationships when linear models fail.

Researchers analyze various statistical indices to compare multiple models, systematically assess their strengths and weaknesses, and ultimately determine the most effective method for their analysis. This study utilizes the coefficient of determination (R^2), root mean square error (RMSE), and mean absolute error (MAE) to evaluate the performance of regression models. The equations of these indices are shown below:

$$R^2 = 1 - \left(\frac{\sum_{i=1}^{n}(y_m - y_p)^2}{\sum_{i=1}^{n}(y_m - y_a)^2}\right) \quad (1)$$

$$\text{RMSE} = \sqrt{\frac{1}{n}\sum_{i=1}^{n}(y_m - y_p)^2} \quad (2)$$

$$\text{MAE} = \frac{1}{n}\sum_{i=1}^{n}\left|y_m - y_p\right| \quad (3)$$

Where y_m: is the measured value, y_p: is the predicted value, y_a: is the average of the measured value, and n: is the total number of data.

These metrics offer a comprehensive insight into the model's performance. The R^2 coefficient of the regression model is used to quantify the variability in the dataset that the model explains. A value close to one indicates a good fit, as the model represents the relationship between the variables very well. MAE measures the average size of the differences between the observed and predicted values; smaller values represent higher accuracy and, therefore, higher reliability of the estimates of the predicted values. RMSE quantifies the standard deviation of the differences between observed and predicted values, providing a

measure of the model's prediction accuracy. Lower RMSE values indicate that the prediction errors are smaller and more consistent, signifying greater precision in the model's performance.

The more predictors are added to the MLR model, the more accurate it becomes; however, this can also introduce additional potential challenges, such as Multicollinearity and overfitting. Overfitting occurs when the model becomes too complex and starts to fit noise in the dataset, which decreases the model's performance on other datasets. In the case of multicollinearity, predictor variables that are too highly correlated with each other make it impossible to differentiate which of them is influencing the dependent variable, resulting in false model results.

This study employed the Variance Inflation Factor (VIF) calculated using SPSS software to assess multicollinearity among the independent variables. VIF detects a correlated predictor that reduces the stability and accuracy of the regression model. Multicollinearity problems, indicated by VIF values of less than 1 or greater than 10, suggest that some variables may be providing redundant information. This redundancy only leads to a loss of interpretation and predictive capacity of the model. Table 3 shows the VIF values for four independent variables: DD, UPV, LRH, and Rn. The VIFs for LRH, DD, Rn, and UPV are 3.90, 3.96, 4.91, and 4.51, respectively. All of the VIF values recorded are less than 10, indicating that there is no multicollinearity problem in this dataset. The moderate values of these independent variables show that they are specifically different and valuable to the regression model, thus increasing the stability of the results. UPV has the highest VIF of 4.909, but this value falls within acceptable limits, indicating that the presence of such correlation with other predictors doesn't affect the model's integrity. The regression model can work well without any concerning multicollinearity, as the data suggests.

Table 3
Predictors' Variance Inflation Factor (VIF).

Independent Variables	Collinearity Statistics VIF
LRH	3.90
DD	3.96
R_n	4.91
UPV	4.51

Correlation coefficients between UCS and the independent variables are shown in Table 4, indicating a strong positive relationship among these variables. These results highlight the interdependence of these parameters and their importance in describing material properties, and LRH and DD are shown to be particularly strong individual predictors of UCS.

Table 4
Correlation matrix for the selected independent variables.

	UCS	LRH	DD	Rn	UPV
UCS	1.00	0.88	0.86	0.84	0.86
LRH	0.88	1.00	0.79	0.82	0.83
DD	0.86	0.79	1.00	0.84	0.80
R_n	0.84	0.82	0.84	1.00	0.84
UPV	0.86	0.83	0.80	0.84	1.00

2.4. Proposed long short-term memory (LSTM) method

This study employs LSTM networks to forecast the UCS and Et using a defined set of input parameters. LSTMs are an advanced form of RNN engineered to handle sequential data by preserving information over prolonged durations. This renders them especially efficient for tasks where the interrelations among input features—such as Leeb rebound hardness, dry density, ultrasonic pulse velocity, and Schmidt hammer

rebound values—may change over time. The architecture of LSTMs is designed to address issues associated with sequence learning, particularly the vanishing gradient problem that frequently affects traditional RNNs. An LSTM unit consists of three essential components: the input gate, the forget gate, and the output gate.

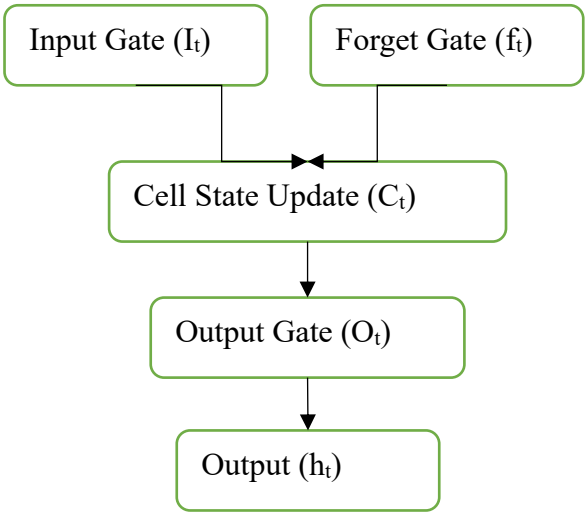

Fig. 4. LSTM block diagram.

The forget gate determines which information from the preceding cell state should be eliminated. It is computed utilizing a sigmoid activation function as follows:

$$f_t = \sigma\left(W_f \cdot [h_{t-1}, x_t] + b_f\right) \tag{4}$$

Where σ is the sigmoid activation function,W_f represents the weight matrix for the forget gate, h_{t-1} is the previous hidden state, x_t is the current input, and b_f is the bias.

The input gate controls the new information to be added to the cell state. It consists of two parts: the input gate itself and a candidate cell state, defined by:

$$i_t = \sigma(W_i \cdot [h_{t-1}, x_t] + b_i) \tag{5}$$

$$\tilde{C}_t = tanh(W_c \cdot [h_{t-1}, x_t] + b_c) \tag{6}$$

Here, $i_t$determines what portion of the new information to store while $\tilde{C}_t$ provides a candidate value that can be added to the state. The cell state is updated by combining the retained information from the previous state with the new input:

$$C_t = f_t \cdot C_{t-1} + i_t \cdot \tilde{C}_t \tag{7}$$

This allows the network to maintain relevant information over time. Lastly, the output gate regulates what part of the cell state will be output to the next layer, calculated as follows:

$$O_t = \sigma(W_o \cdot [h_{t-1}, x_t] + b_o) \tag{8}$$

$$h_t = O_t \cdot \tanh(C_t) \tag{9}$$

The output h_t is determined by applying an activation function to the cell state, modulated by the output gate. This structure enables the LSTM to effectively manage information flow, making it highly suitable

for tasks involving sequential data. Fig. 4 is a block diagram illustrating the flow of information in an LSTM unit, which supports the explanation of the equations mentioned:

3. Test Result and discussion

3.1. Test result

LRH, Rn, DD, UPV, UCS, and Et tests were conducted on 134 rock samples cored from 134 rock boulders in the study area. Test results and statistical parameters are presented in Fig. 5. The average of the UCS is 91.2 MPa and varies between 51.95 and 91.95 MPa, while the average value of Et is 18.0 GPa and ranges between 11.89 and 24.89 GPa; based on these values, this rock is classed as strong to very strong rock according to EN ISO 14689 [48] and (CH to BH). According to [49], the average dry density is about 2.553 g/cm^3 and varies between 2.412 and 2.689 g/cc, and based on the International Aerospace Environmental Group (IAEG), these rocks are classified as classes 3 and 4 (moderate to high density). The IAEG proposed a classification criterion for rock based on ultrasonic pulse velocity. Based on this criterion, the study samples varied from low to very high wave velocity.

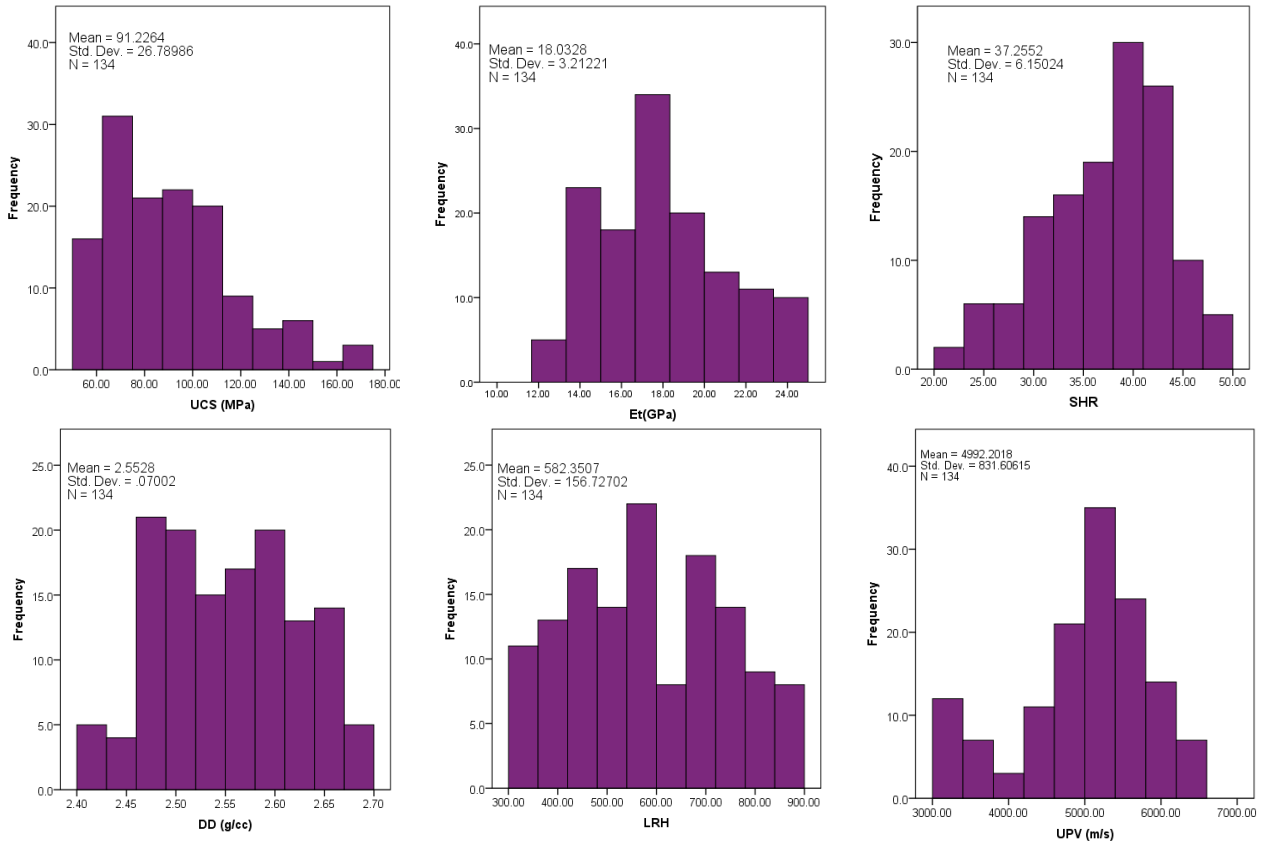

Fig. 5. Distribution of test results; a) UCS, b) LRH, c) Rn, d) DD, e) Et.

3.2. Predicting UCS using simple regression analysis

Simple regression is a widely used approach among researchers to predict UCS from nondestructive test results [47,50–52]. This method results in an inexpensive and efficient estimation of rock strength.

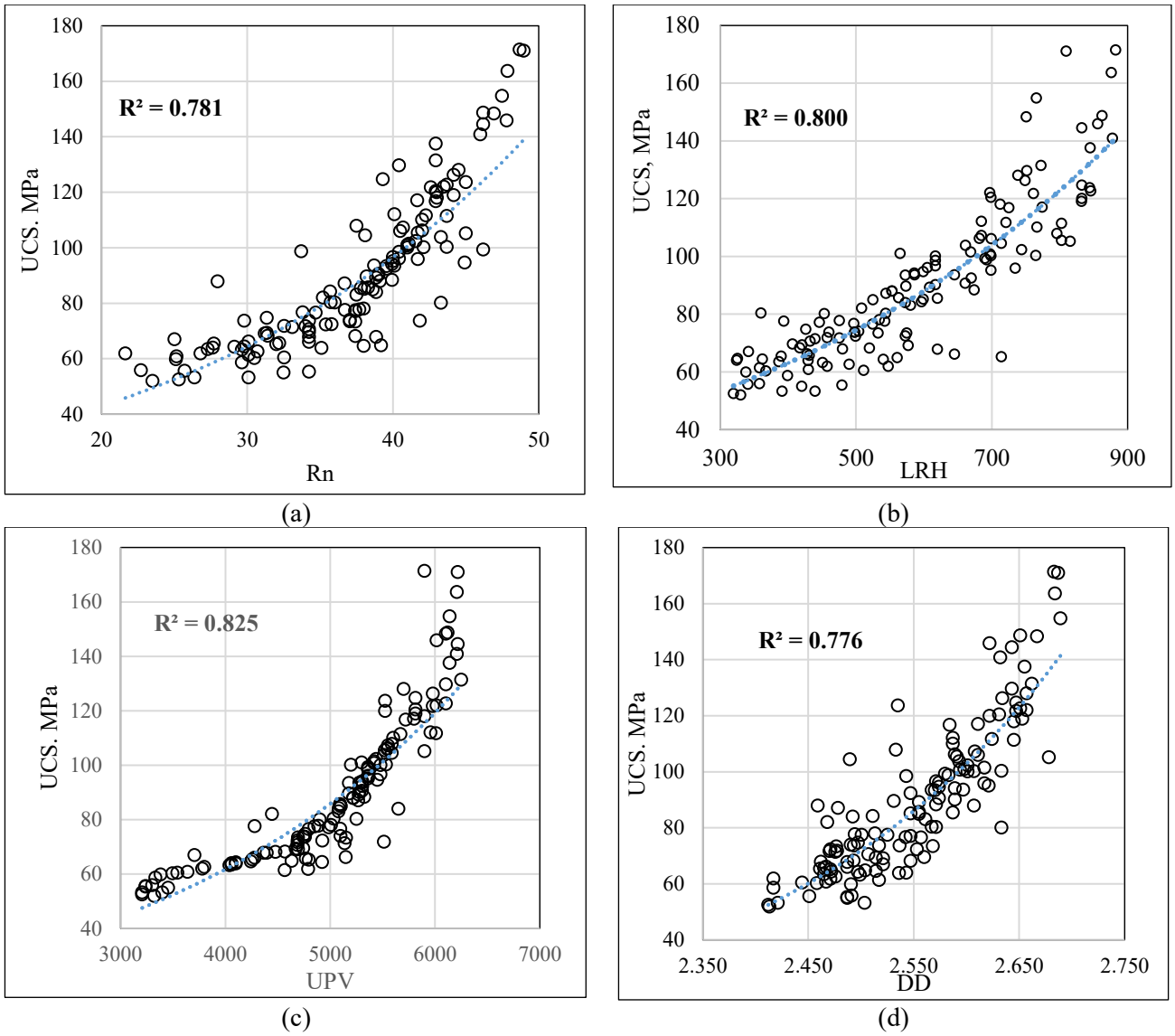

Fig. 6. The developed equations for estimating UCS using (a) Schmidt hammer rebound number, (b) Leeb rebound hardness, (c) P-wave velocity, and (d) Dry density.

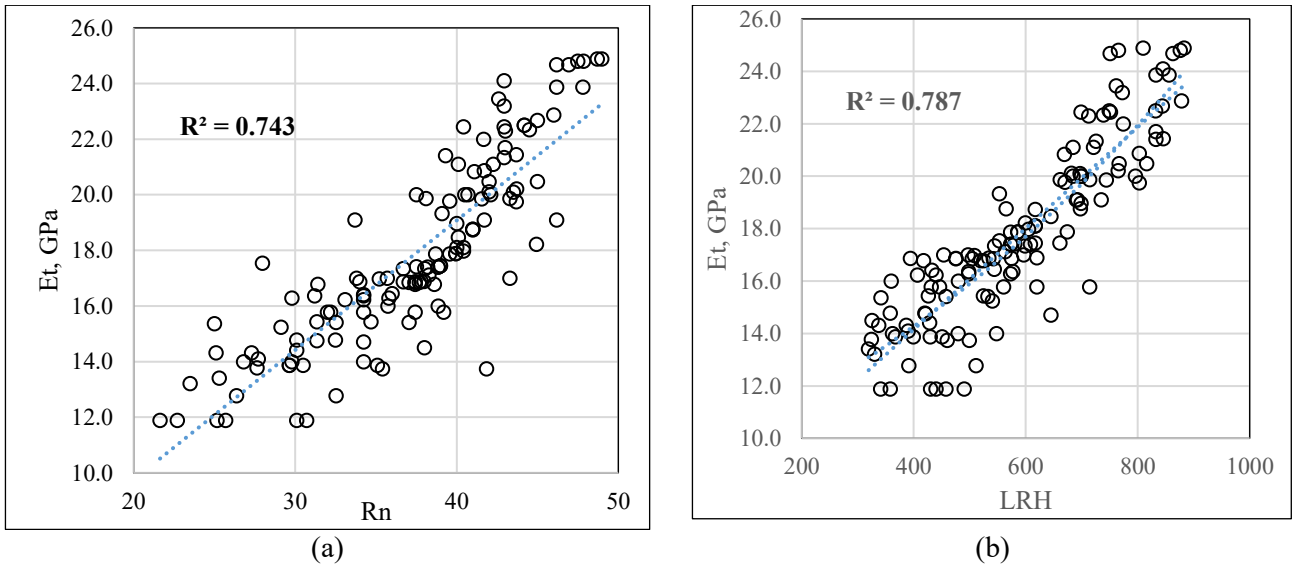

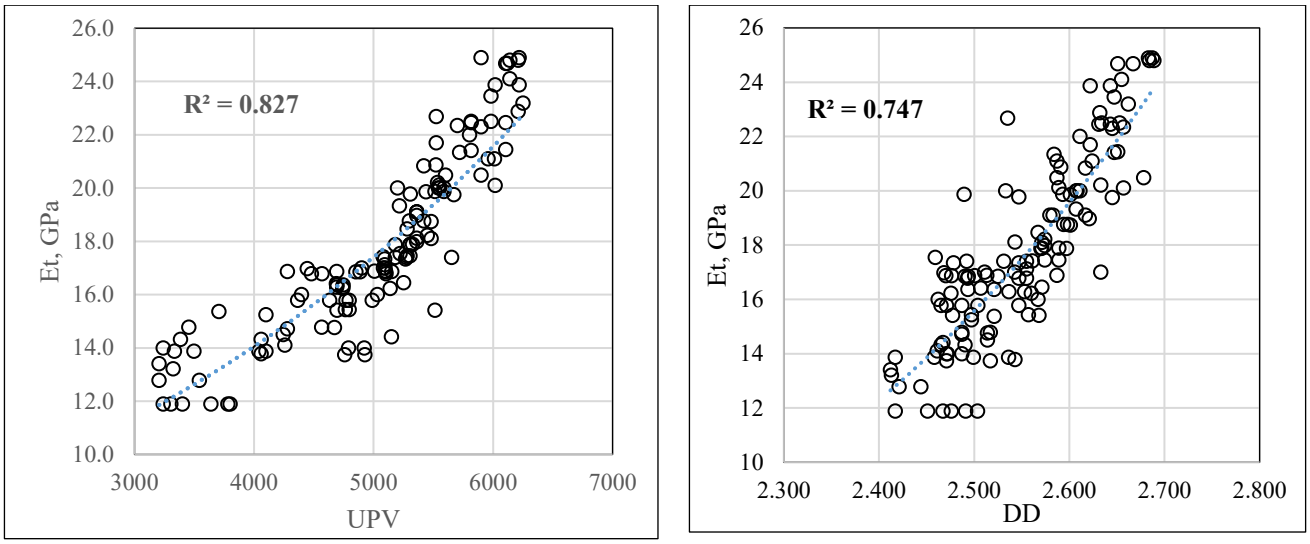

(c) (d)

Fig. 7. The developed equations for estimating Et using (a) Schmidt hammer rebound number, (b) Leeb rebound hardness, (c) P-wave velocity, and (d) Dry density.

In this study, UCS and Et were used as dependent variables, while DD, UPV, Rn, and LRH were used as independent variables. Linear, power, exponential, and logarithmic regression analyses were performed between UCS and each index parameter. The efficiency of the predicted simple regression equations was statistically assessed using performance indices R^2, RMSE, and MAE, and the optimal equation to estimate UCS and Et was identified.

Figs. 6 and 7 show the scatter plot of the data points, where the x-axis represents the independent variable and the y-axis represents the dependent variable. Data dispersion and clustering can reveal the nature and strength of the relationship between the variables.

Table 5 shows the relationships between UCS and Et as dependent variables, with independent variables (DD, RH, LRH, and UPV). The correlation equations are used to represent these relationships, and their quantitative evaluation is performed using statistical metrics such as R^2, RMSE, and MAE. R^2 values from ranges 0.776 to 0.825 for DD to UPV, respectively, showing strong correlations across all variables for UCS predictions.

The most reliable predictor of UCS is UPV, with the highest R^2 (0.825). Furthermore, in terms of error metrics, UPV is lower in RMSE (12.97) and MAE (9.42) compared to other variables, indicating that it is the most reliable predictor of UCS. A high R^2 value (0.80) and the lowest MAE (8.89) indicate that LRH is another strong predictor. R^2 values for DD and RH are reasonable (0.776 and 0.781, respectively), but their higher RMSE and MAE indicate slightly less precise predictions of UCS.

The R^2 values for Et predictions are 0.743 for RH and 0.825 for UPV, which are comparable to those for UCS. Again, UPV is the strongest predictor with the highest R^2. Additionally, it has the lowest RMSE (1.48) and MAE (1.13) among models for predicting Et. An R^2 of 0.787 and competitive RMSE (1.54) and MAE (1.20) are achieved by LRH closely. On the other hand, DD and RH have slightly lower R^2 (0.747 and 0.743, respectively) and higher RMSE and MAE for predicting Et than UPV and LRH. In terms of both UCS and Et prediction, UPV shows the best prediction performance.

LRH is a strong secondary predictor for both UCS and Et. DD and RH are still useful for standalone prediction, but they have lower correlation and higher error metrics. However, the accuracy and reliability of predictions may be further improved by multivariate analysis of multiple variables.

Table 5
Best fit function for the independent variables.

Dependent	Variable	Correlation Equation	R^2	RMSE	MAE
UCS	DD	$UCS=0.009*e^{3.574DD}$	0.776	14.09	10.30
	Rn	$UCS=19.083\ e^{0.0405*Rn}$	0.781	12.99	9.49
	LRH	$UCS=32.38\ e^{0.002LRH}$	0.80	12.15	8.89
	UPV	$UCS=16.525\ e^{0.00031*UPV}$	0.825	12.97	9.42
Et	DD	$Et=0.758xDD^{5.8126}$	0.747	1.68	1.31
	Rn	Et=0.4662xRH+0.4292	0.743	1.69	1.34
	LRH	$Et=0.0193x^{LRH+6.435}$	0.787	1.54	1.20
	UPV	$Et=5.97*e^{0.00021*UPV}$	0.827	1.48	1.13

3.3. Multiple linear regression (MLR)

MLR analysis was used in his study to examine relationships between UCS, Et and multiple independent variables. A simple bivariate correlation analysis was conducted to assess the strength of the relationships between UCS and each of the independent variables. In this case, Table 6 shows that the Pearson Correlation coefficient was used to quantify these relationships.

Results show that UCS is positively correlated with independent variables to varying degrees. For example, DD exhibits a weak positive correlation with UCS, a medium positive correlation with UPV, and strong positive correlations with PL, RH, and LH. These findings help justify the inclusion of these predictors in the MLR analysis and show their relative importance. The study considers all independent variables, ensuring that all factors influencing UCS are thoroughly investigated.

Table 6
Correlation values of independent variables with UCS.

Independent Variables	**Pearson Correlation**	
	UCS	Et
LRH	0.878	0.887
DD	0.859	0.857
UPV	0.862	0.885
Rn	0.844	0.862

The stepwise MLR table illustrates the successive development of regression models to predict UCS by stepwise addition of independent variables (LRH, DD, and UPV) as shown in Table 7. In Model 1, LRH is the only predictor, with an R^2 of 0.771, accounting for 77.1% of the variability in UCS, and showing strong statistical significance ($t = 21.072$, $p < 0.001$). There is no multicollinearity (VIF = 1.000). In model 2, the model's explanatory power is greatly increased by the addition of DD, which increases R^2 to 0.846. LRH and DD remain highly significant ($p < 0.001$) and have acceptable VIF values (2.609) with no significant multicollinearity. In model 3, the R^2 was improved to 0.864, and the predictors (LRH, DD, UPV) are statistically significant ($p < 0.001$), and VIF values are less than 5 (acceptable collinearity). The result of the stepwise MLR model suggests that Rn was not included in the model as it did not satisfy the inclusion criteria during the regression process. Variables are added in stepwise regression only if they significantly improve the model's predictive power. Moreover, Rn could be highly correlated with one or more of the existing predictors, resulting in multicollinearity, where the model gives preference to the variables that explain the most variance independently.

Stepwise development of the regression models predicting Et using independent variables (LRH, UPV, and DD) is summarized in Table 8. In Model 1, LRH is the only predictor, with an R^2 of 0.787, which means that LRH alone accounts for 78.7% of the variability in E_t. LRH ($t = 22.078$, $p < 0.001$) makes a highly significant contribution, with a VIF of 1.000 and no multicollinearity issues. The R^{2-}Value of Model 2

improved to 0.86 with the addition of UPV, which substantially enhances the model's explanatory power. Although the VIF for both variables has increased to 3.152, indicating moderate correlation, LRH ($t = 8.447$, $p < 0.001$) and UPV ($t = 8.289$, $p < 0.001$) remain highly significant. DD is included in Model 3, and the R^2 value is 0.884, which further enhances the model. All predictors (LRH, UPV and DD) are statistically significant ($p < 0.001$), and VIF values between 3.262 and 3.941 indicate acceptable levels of multicollinearity.

Similar to the UCS prediction, R_n did not satisfy the inclusion criteria and was not included in the stepwise regression model. The exclusion of R_n means that it did not significantly contribute to the model's performance, which is due to the fact that stepwise regression optimizes explanatory power, keeping statistically significant variables first.

Table 7
The UCS Model Summary.

Model		Unstandardized Coefficients		t	Sig.	F	R	R Square	VIF	Durbin-Watson
		B	Std. Error							
1	(Constant)	-1.108	4.479	-0.247	0.805	444.05	0.878	0.771		
	LRH	0.155	0.007	21.072	0.000				1.000	
2	(Constant)	-400.38	50.206	-7.975	0.000					
	LRH	0.094	0.010	9.576	0.000	359.09	0.920	0.846	2.609	
	DD	170.621	21.397	7.974	0.000				2.609	0.894
3	(Constant)	-325.33	50.708	-6.416	0.000					
	LRH	0.070	0.011	6.426	0.000	274.7	0.929	0.864	3.621	
	DD	128.77	22.570	5.705	0.000				3.262	
	UPV	0.009	0.002	4.145	0.000				3.941	

a. Dependent Variable: UCS
b. Predictors: (Constant), LRH
c. Predictors: (Constant), LRH, DD
d. Predictors: (Constant), LRH, DD, UPV

Table 8
The MLR Models Summary for ET estimation.

Model		Unstandardized Coefficients		t	Sig.	F	R	R Square	VIF	Durbin-Watson
		B	Std. Error							
1	(Constant)	6.437	0.533	12.077	.000	487.4	0.887[a]	0.787		
	LRH	0.019	0.001	22.078	.000				1.000	
2	(Constant)	1.341	0.752	1.784	.077					
	LRH	0.011	0.001	8.447	.000	403.1	0.927[b]	0.860	3.152	
	UPV	0.002	0.000	8.289	.000				3.152	1.334
3	(Constant)	-28.072	5.780	-4.856	.000					
	LRH	0.008	0.001	6.763	.000	329.3	0.94[c]	0.884	3.621	
	UPV	0.001	0.000	5.804	.000				3.941	
	DD	13.186	2.573	5.125	.000				3.262	

a. Predictors: (Constant), LRH
b. Predictors: (Constant), LRH, UPV
c. Predictors: (Constant), LRH, UPV, DD
d. Dependent Variable: Et

A homoscedasticity test was conducted to see whether the residuals of the regression model were equally distributed. Homoscedasticity implies that the variance of residuals is constant at all levels of the predicted values, a necessary condition for the validity of predictions. The residuals are approximately normally distributed, as shown in Figures 8 and 9; that is, they are randomly distributed around zero with no obvious pattern or systematic deviation. This result confirms that the model satisfies the homoscedasticity assumption, i.e., that the relationships between the predictors and the dependent variable are stable and unbiased in the range of the data.

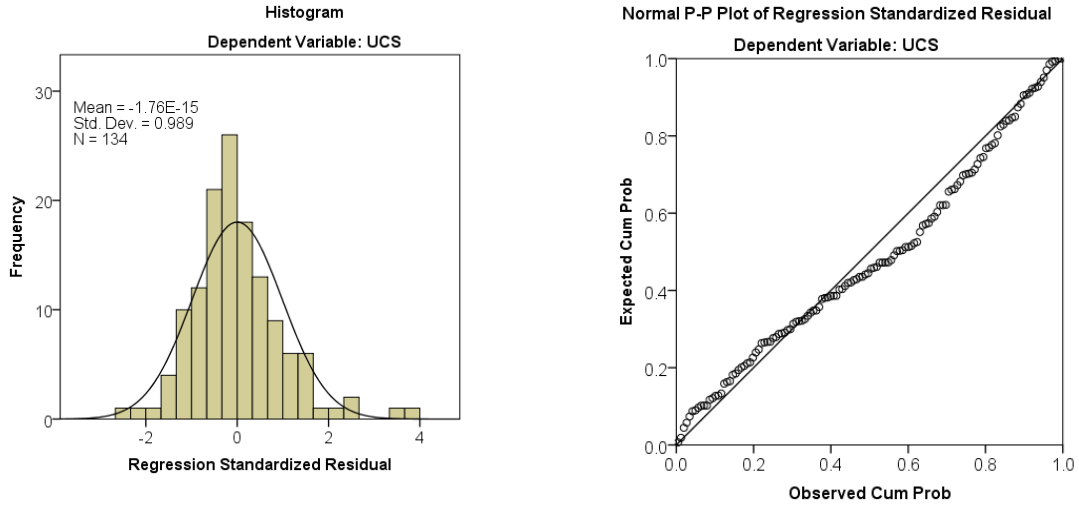

Fig. 8. Frequency and P-P Plots of the Standardized Residual for the UCS dependent variable.

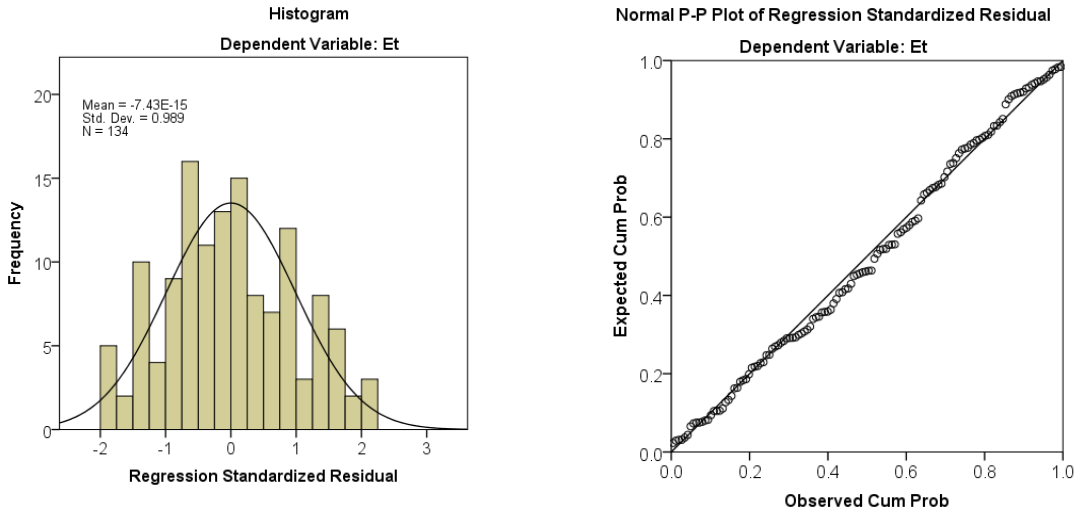

Fig. 9. Frequency and P-P Plots of the Standardized Residual for the E_t dependent variable.

The Durbin-Watson (DW) statistical method is used to detect the presence of serial correlation in the residuals of a regression model. If residuals are not independent of each other, then the residuals exhibit serial correlation, and this can undermine the validity of the regression analysis. In this study, the DW value is 0.89, which is below the acceptable range of 1.5 to 2.5, indicating significant positive serial autocorrelation in the residuals. This result implies that the residuals are not independent because of a very high positive autocorrelation, and thus, the regression model's findings may not be entirely reliable.

For low DW values (i.e., significant positive autocorrelation in residuals), LSTM networks are a feasible modeling option. The LSTMs are specifically designed to identify sequential patterns and temporal relationships in the data, thereby addressing the autocorrelation issue through their built-in data structure.

Additionally, LSTMs are well-suited for modeling nonlinear dependencies, as residual dependencies are often present to enhance the predictive accuracy and performance of the model.

3.4. NLR results

Different nonlinear models were generated. Equation 10 represents the best nonlinear model for predicting UCS.

$$UCS = 2.294 \times e^{0.848DD} \times e^{0.01025Rn} \times e^{0.00015UPV} \times e^{0.00055LRH} \quad (10)$$

The analysis of the nonlinear regression prediction for UCS revealed that the best model was developed using four predictors, with an R^2 of 0.92 and a minimum RMSE of 7.59. Fig. 10 visually represents the goodness of fit achieved by the developed models. The analysis of the results showed that, in terms of predictive capability and the capacity to explain variation in the UCS, nonlinear regression is slightly better at predicting and explaining variation in UCS values than MLR. Using the nonlinear regression approach enhanced the model strength by only 6% for the models predicting the UCS using four predictors. However, the use of the nonlinear regression approach enhances the model's strength and accuracy of predictions, as expected from utilizing nonlinear associations.

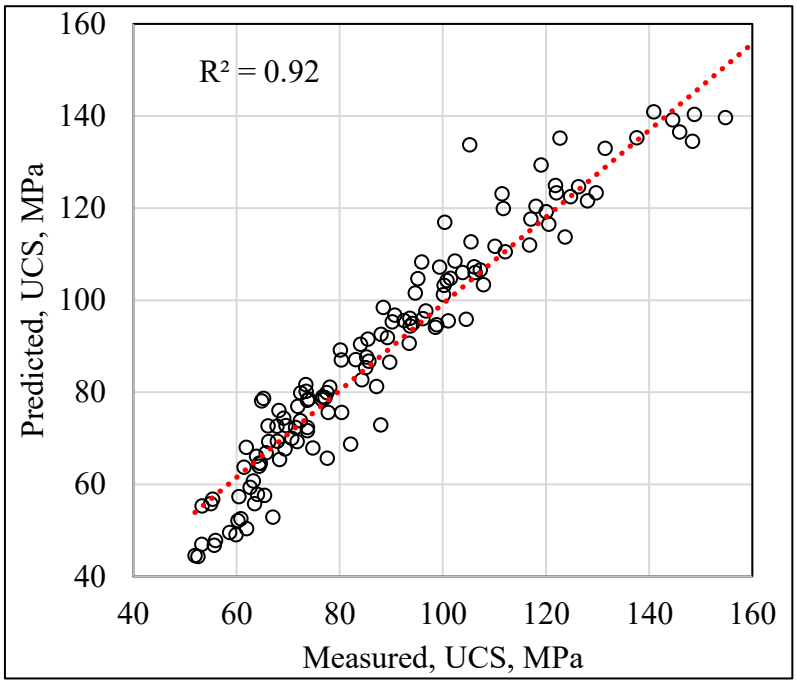

Fig. 10. Nonlinear model results for UCS Prediction.

Several nonlinear models were also developed to assess the effectiveness of Et prediction. Of these models, Equation 11 was the one that best predicted the data and best aligned with the observed data.

$$E_t = DD^{0.389} \times e^{0.00866Rn} \times (0.00257 \times LRH + 4.989) \times e^{6.47\times10^{-5}UPV} \quad (11)$$

The analysis shows that a nonlinear regression using four predictors yields higher performance, with an R^2 of 0.90 and a minimum RMSE of 1.12, thus explaining and predicting the variations in Et very well. Fig. 11 visually represents the goodness of fit achieved by the developed models. Results show that nonlinear regression gave a small additional improvement in predicting and explaining the variation in Et values over

MLR, with the R^2 value increasing from 0.88 to 0.90. This implies that nonlinear regression fits slightly better and explains slightly more of the variance in Et. However, although nonlinear regression can explain more complex relationships between variables, adding complexity to the nonlinear model did not significantly improve the prediction of the linear model.

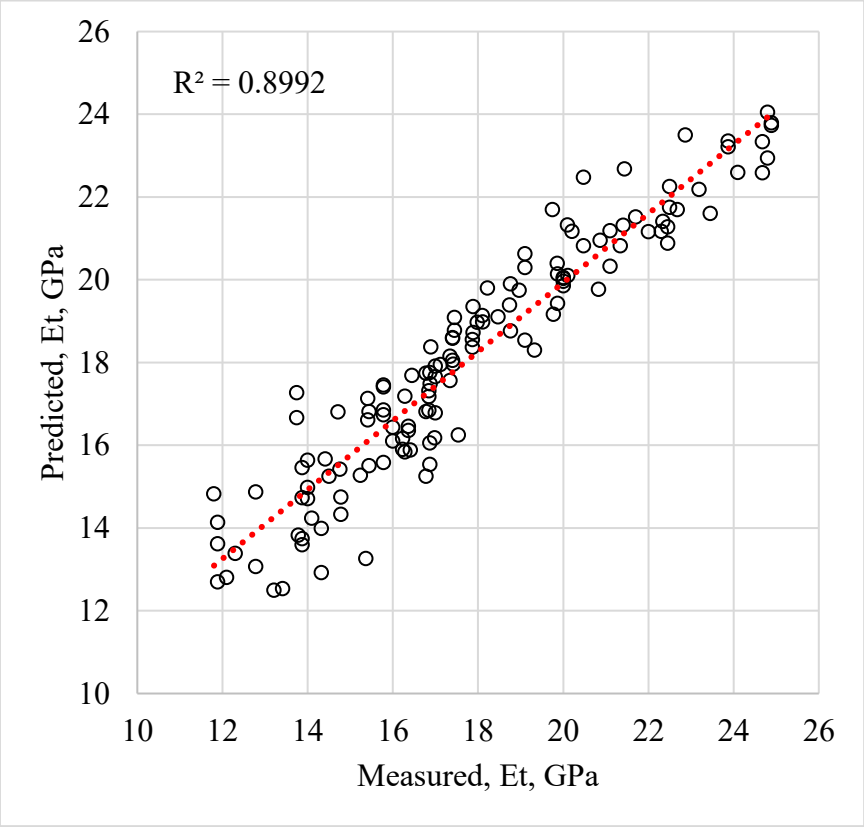

Fig. 11. Nonlinear model results for Et Prediction.

3.5. LSTM network configuration and results discussion

The model architecture features a sequence input layer that processes the four input parameters, followed by an LSTM with 100 units, which generates the final hidden state, and a fully connected layer to predict the predicted value of UCS or Et. Several hyperparameters were fine-tuned to improve training efficiency. A mini-batch size of 10 was employed for efficient gradient updates, and a learning rate of 0.001 was used to facilitate stable convergence. Furthermore, a piecewise learning rate schedule with a learning rate drop factor of 0.5 and a learning rate drop period of 10 was also used to adjust the learning rate systematically during training. The dataset is divided into a training and a test set with an 80:20 ratio. A random division is employed, followed by normalization. During the experiment, the separation of the test dataset is ensured, preventing its impact on the training phase.

Each feature in the dataset is individually normalized as part of preparing the LSTM model for training. This step holds significance because input features such as LRH, DD, UPV and Rn can differ greatly in range. Normalizing data ensures that every input feature equally participates in the learning process, which facilitates and enhances the efficiency of the training process and model convergence. The correlation matrix shown in Table 4 illustrates the coefficients of correlation between various properties of the material, with a specific focus on the relationships between features and target variables. Each cell inside the table measures the degree of relatedness between two variables, which can range from -1 to +1. If the coefficient

is +1, it signifies a perfect positive relation; if it is -1, conversely, that means a perfectly negative link exists; a value of zero would mean no relation is present at all.

After normalizing the data, it is split into two sets: training and testing. The training set is used to train the LSTM model, and the testing set is reserved for evaluating the model's performance. The model optimizes prediction errors on training. At each training step or epoch, the progress of the RMSE is tracked. Training is performed, and RMSE values are recorded as the training progresses to monitor the model's improvement. As shown in Fig. 12, the RMSE decreases steadily as the model learns and becomes more accurate, indicating a lower RMSE that confirms the improvement in predictions.

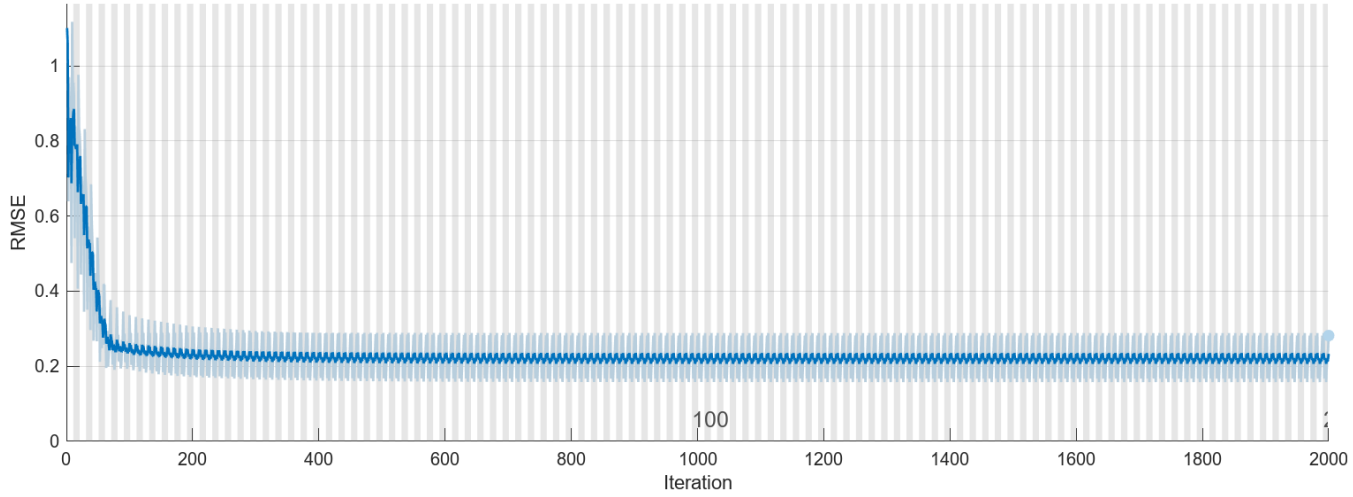

Fig. 12. RMSE over the iterations during training of the LSTM network.

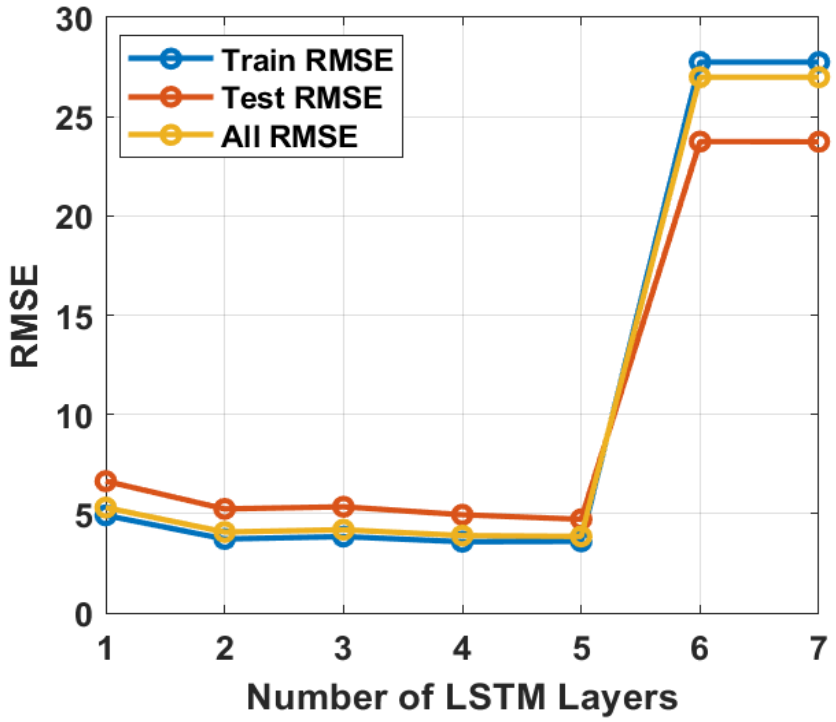

Fig. 13. RMSE over the number of LSTM layers.

Determining the optimal number of layers in an LSTM architecture is crucial, as it influences the model's capacity to learn complex patterns while maintaining generalization. An inappropriate number of layers can result in either underfitting or overfitting, thus adversely affecting predictive accuracy. Therefore, LSTM is

initially configured with varying layers, and RMSE is analyzed to determine the optimum number of layers in LSTM. The plot in Fig. 13 illustrates the RMSE against the number of LSTM layers and provides critical insights into the model's performance across varying complexities. Initially, as the number of LSTM layers increases from one to five, both the training and testing RMSE values remain relatively stable, indicating effective model training and generalization. This stability suggests that the model adequately captures the underlying patterns in the data without significant overfitting. However, a noticeable spike occurs at six LSTM layers, where the RMSE values for both training and testing datasets escalate dramatically, indicating a deterioration in model performance. This increase suggests that the model may have become overly complex, leading to overfitting and a subsequent failure to generalize effectively to unseen data. To thoroughly assess the predictive capabilities of the created models, a wide range of statistical and engineering-based metrics was used. Besides the standard evaluation indices, i.e., MAE, RMSE, and R^2, several other performance indicators have also been computed to understand better the accuracy, robustness, and reliability of the models. These include the Performance Index (PI), which integrates error magnitude and variability; the A-10 Index, which quantifies the percentage of predictions falling within ±10% of the actual values; Theil's Inequality Coefficient (TIC), an efficiency measure of a model against a naive forecast; the Index of Agreement (IA), a normalized measure of predictive precision; and the Stability Index (SI), that shows the consistency of the model output at different data points [53–57]. To get a scale-independent analysis of error, R2 is calculated. It represents the proportion of the variance in the target. The weakness of R2 is its incrementation by adding predictors. Therefore, an adjusted R2 score (A-10) was used, which increases if newly added predictor features improve the model. Table 9 lists equations to calculate these parameters.

Table 9
Formulas for quantitative matrices.

Matrices	Best Performance	Equation	no
Performance Index	Low	$PI = \frac{RMSE}{n \times \sqrt{R^2 + 1}}$	(12)
TIC	Low	$TIC = \sum_{i=1}^{n} \left\| \frac{y_{p,i} - y_{m,i}}{y_{m,i}} \right\|$	(13)
Sensitivity Index	Higher	$SI = \frac{2 \times \sum_{i=1}^{n} \min(y_{p,i}, y_{m,i})}{\sum_{i=1}^{n} y_{p,i} + \sum_{i=1}^{n} y_{m,i}}$	(14)
A-10	Unity	$A10 = 1 - \left(\frac{1 - R^2}{n - k - 1}\right)(n - 1)$	(15)
Index of Agreement	Unity	$IA = 1 - \frac{\sum_{i=1}^{n} \left(y_{p,i} - \mu_{y_p}\right)^2}{\sum_{i=1}^{n} \left(\left\|y_{p,i} - \mu_{y_p}\right\| + \left\|y_{m,i} - \mu_{y_m}\right\|\right)^2}$	(16)

The predicted values of the target variable, UCS, for the training and test datasets were plotted. An assessment of the model's accuracy can be made directly from this visualization, comparing the model's predictions to the observed values. The train and test dataset prediction and comparison with actual target values are shown in Figs. 14 and 15. The mean errors for the predicted target values of both the training

and test datasets align with the results, indicating that for the training set, the mean error was -0.13, and for the test set, the mean error was -3.52 for the UCS. Likewise, the error means for 0.0009 and -0.27, respectively, for the training and testing datasets of the Et, likewise exhibit strong alignment with the greater model's performance.

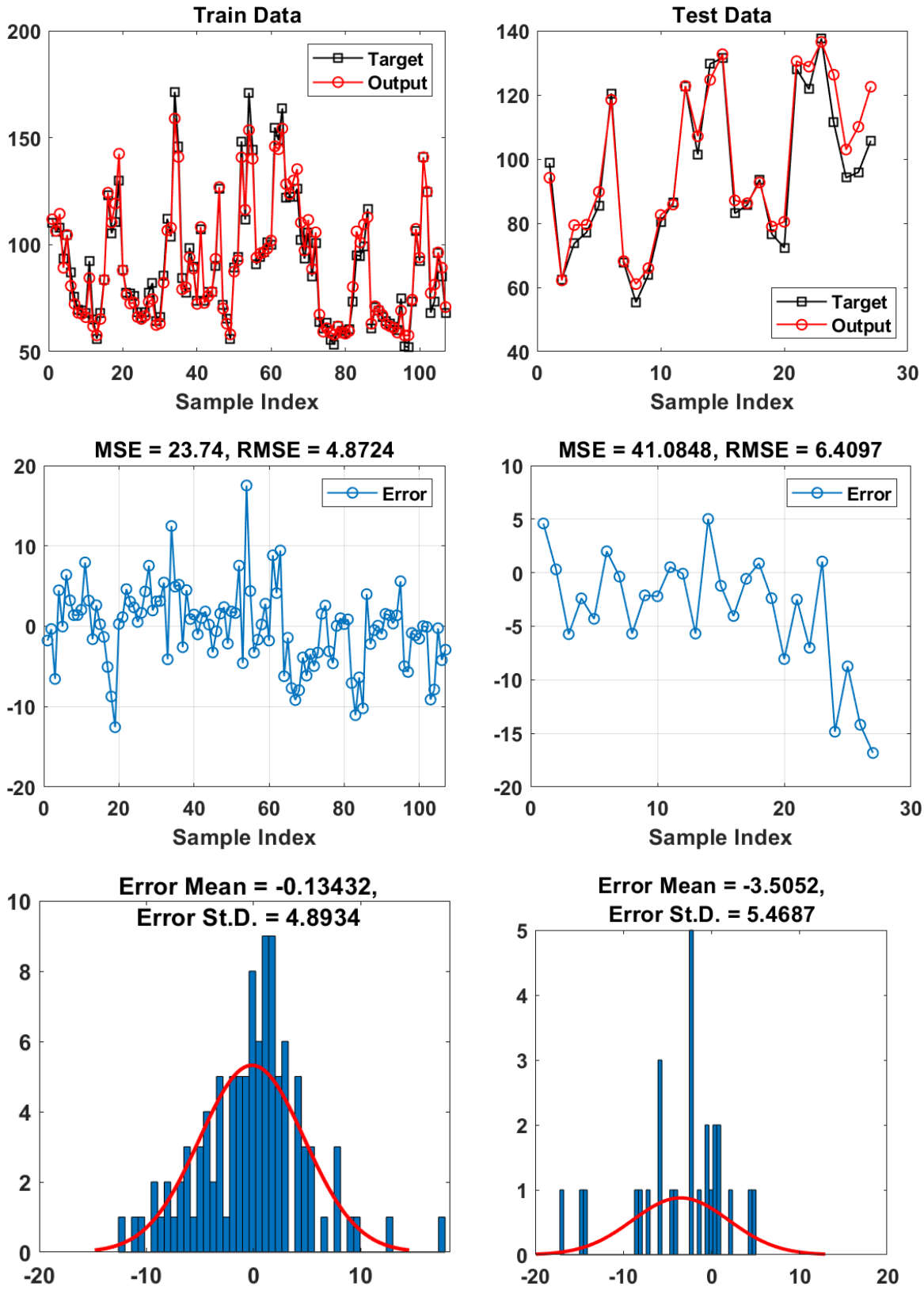

Fig. 14. LSTM prediction and error analysis for training and test datasets, Uniaxial comprehensive strength.

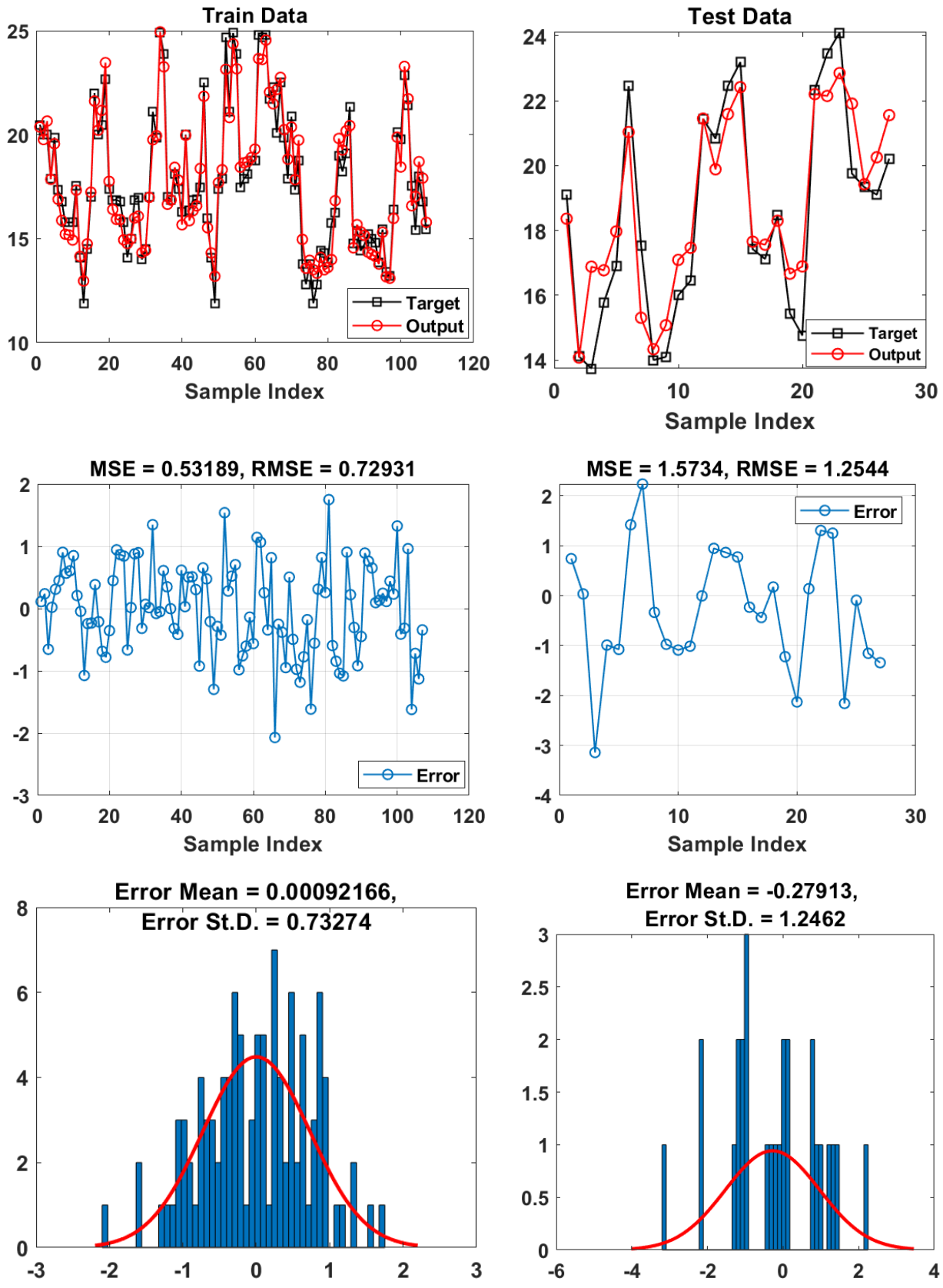

Prediction using the training dataset Prediction using the test dataset

Fig. 15. LSTM prediction and error analysis for training and test datasets, Et.

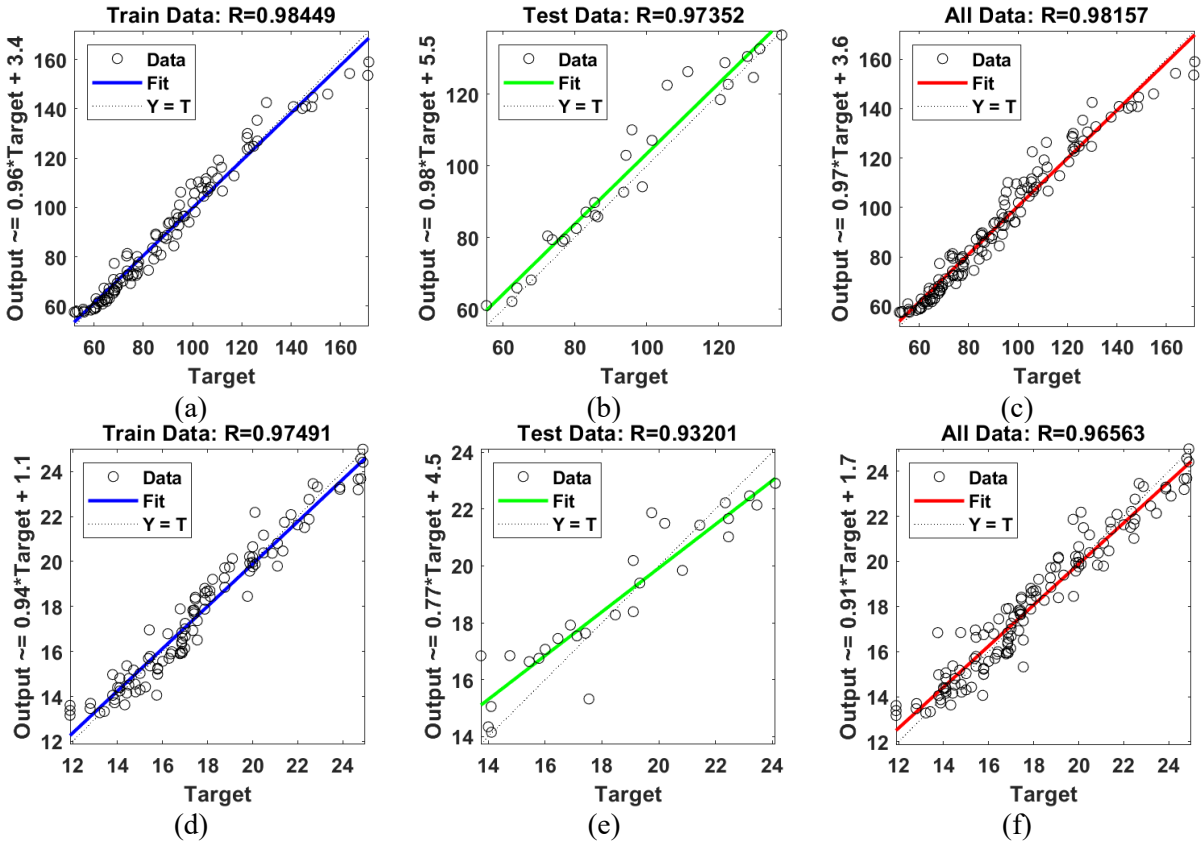

Fig. 16. R^2 Score for training, testing, and all datasets of UCS and Et.

Table 10 presents a comprehensive overview of the model's performance metrics for predicting UCS and the Et across training, testing, and combined datasets. The model exhibits commendable performance, as evidenced by a high R2 score and lower RMSE and error means in the prediction, as shown in Fig. 16. We compared the performance of an LSTM model with traditional machine learning approaches, specifically XGBoost and Random Forest (RF).

Both XGBoost and RF models were initialized with their default hyperparameters to establish a baseline performance, ensuring a fair comparison with the LSTM architecture. The evaluation was conducted using a normalized dataset to maintain consistency in feature scaling across all models.

Table 10
Summary of the model's prediction performance using quantitative matrices.

	LSTM			XGboost			RF		
UCS									
	Train	Test	All	Train	Test	All	Train	Test	All
RMSE	4.872	6.409	5.313	4.911	4.877	4.904	4.467	4.703	4.516
R2	0.984	0.973	0.981	0.966	0.962	0.966	0.972	0.965	0.971
Error mean	-0.134	-3.505	-0.826	-0.190	-2.291	-0.613	-0.093	0.753	0.077
ET									
RMSE	0.729	1.254	0.722	0.634	1.217	0.787	0.658	0.879	0.708
R2	0.974	0.932	0.964	0.960	0.866	0.941	0.957	0.930	0.952
Error mean	0.0009	-0.279	-0.076	-0.010	-0.142	-0.037	0.046	0.365	0.110

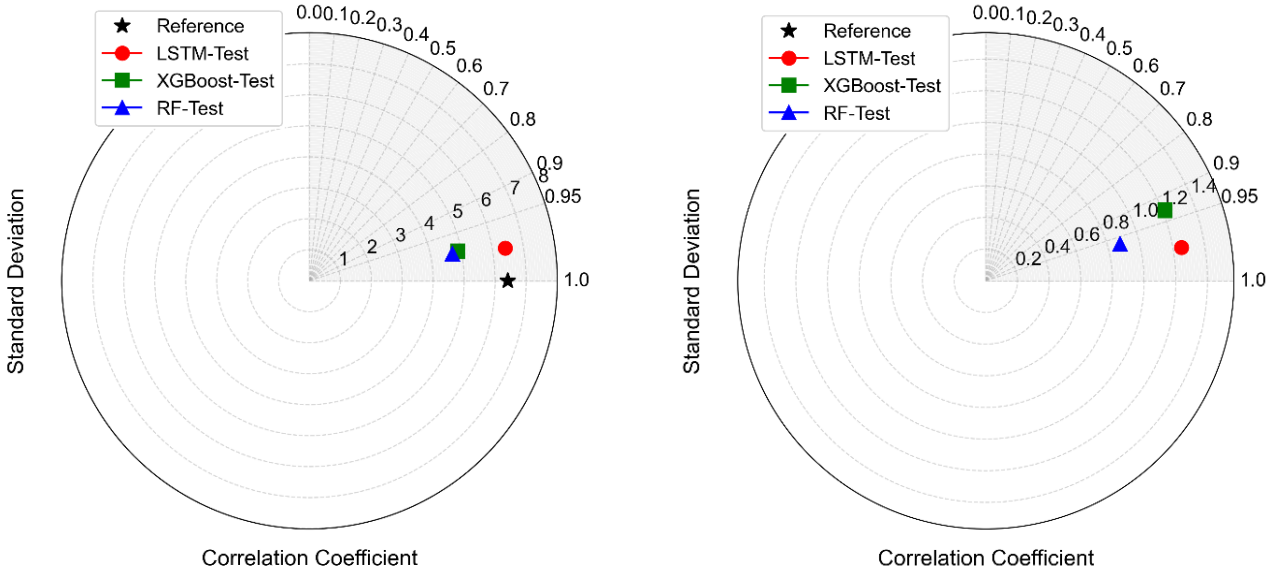

(a) (b)

Fig. 17. Model comparison using Taylor charts (a) For UCS (b) for ET.

The Taylor diagram (Figure 17) effectively synthesizes multiple performance indicators, illustrating the RMSE and correlation coefficients ($\sqrt{R^2}$) relative to a reference model LSTM. Results indicate that while LSTM exhibits higher correlation ($R^2 = 0.973$), XGBoost and RF demonstrate lower RMSE values (4.877 and 4.703, respectively), suggesting a trade-off between error magnitude and explanatory power.

The box plot of prediction errors for the training, test, and overall datasets in Fig. 18 provides a visual representation of the distribution and variability of prediction errors across three subsets of the dataset. The presence of outliers in the test dataset, indicated by points beyond the whiskers, further emphasizes that some predictions deviate slightly from actual values.

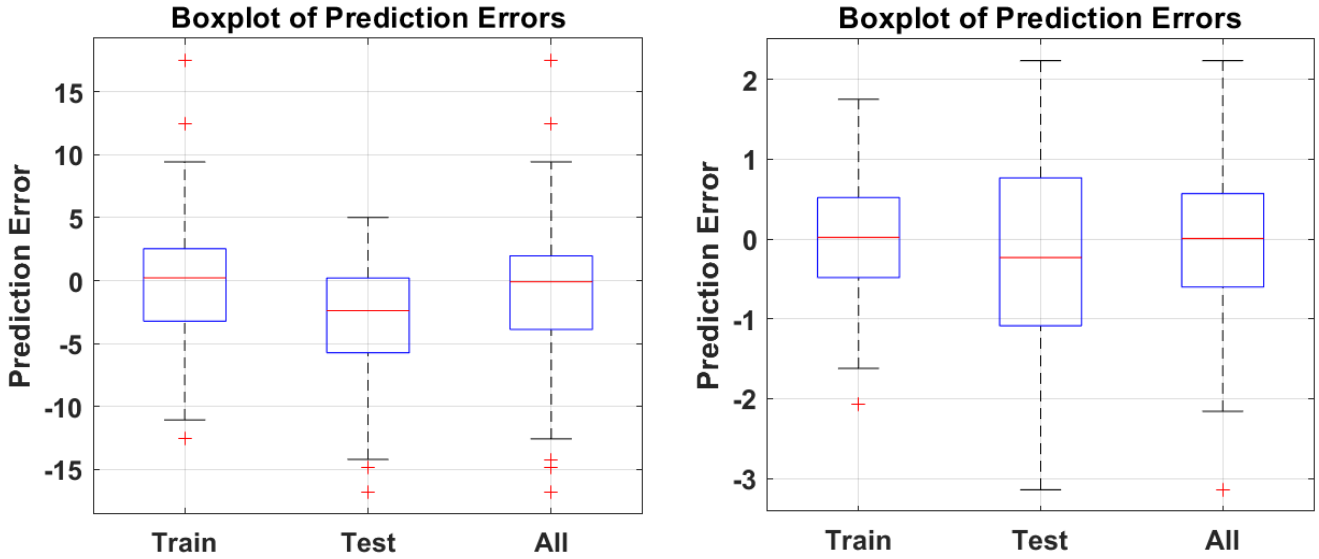

(a)UCS (b) ET

Fig. 18. Prediction error for training, testing, and all data sets using LSTM.

Table 11 shows the additional quantitative parameters evaluated on all datasets. A comprehensive evaluation of LSTM, XGBoost, and RF models for UCS and ET prediction reveals LSTM as the top performer, demonstrating lower PI and TIC, and higher SI, IA, and A-10.

Table 11
Model's evaluation and quantitative parameters comparison.

Metric	Target	LSTM	XGBoost	RF
PI	UCS	0.024	0.0274	0.0261
	ET	0.0038	0.0046	0.0042
A-10	UCS	0.9809	0.9659	0.9711
	ET	0.9634	0.9394	0.9508
TIC	UCS	0.0264	0.0417	0.0386
	ET	0.0274	0.0379	0.0307
SI	UCS	0.9868	0.9792	0.9806
	ET	0.9863	0.9811	0.9846
IA	UCS	0.9928	0.9905	0.9901
	ET	0.9876	0.9813	0.9819

3.6 Sensitivity analysis

The Fourier Amplitude Sensitivity Test (FAST) is an effective technique employed to evaluate the sensitivity of model outputs to independent input parameters. By quantifying both direct and interaction effects, FAST identifies the elements that most significantly influence outcomes, hence directing the decision-making process. Figure 19 shows FAST analysis.

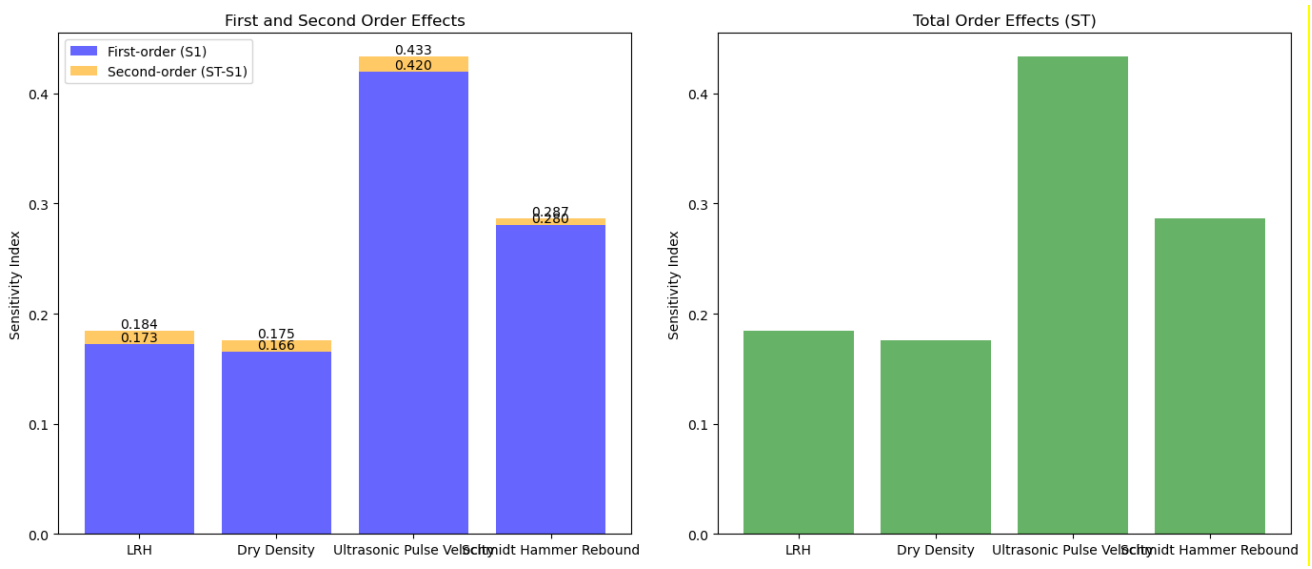

(a) (b)

Fig. 19. Sensitivity indices from FAST analysis (a) First and second order effect (b) Total order effect

In the first plot, the first-order effects indicate the direct influence of each variable on the output. Here, Ultrasonic Pulse Velocity stands out as the most influential factor, with a sensitivity index of 0.433. This suggests that changes in this variable can lead to substantial variations in the output. In contrast, LRH and Dry Density have lower sensitivity indices, indicating they exert a smaller direct influence. The second-order effects reflect the interactions between variables, highlighting how the combined influence of two or more variables can affect the output. The interaction between Ultrasonic Pulse Velocity and Hammer Rebound, for instance, is significant, with a sensitivity index of 0.287.

4. Conclusion

The objective of this study was to present cost-effective and time-efficient methods to predict the rock mechanical properties (UCS and Et) of basalt rocks. Laboratory tests were conducted on 134 rock samples using non-destructive tests, including Leeb rebound hardness, Schmidt hammer, dry density, and ultrasonic

pulse velocity. The data from these tests were used to develop predictive UCS and Et models. Significant correlations were found between UCS, Et and tested results, but the accuracy and effectiveness of the prediction models differed, and the following conclusions were drawn:

Simple regression was used to predict the rock's mechanical properties (UCS and Et) using single predictors, with significantly lower accuracy compared to other methods in this study, as it considered only one independent variable at a time. Simple regression is useful in understanding the relationship between one independent variable and one dependent variable. However, it can, at best, only describe these relationships as a linear function of one variable and is unable to describe the combined effects of other variables or their interactions. As a result, this approach had much lower explanatory power and less model performance than MLR, NLR, and the more advanced LSTM model.

In this study, the MLR analysis successfully identified the relationships between UCS and Et, as well as several independent variables. The explanatory power of the models was improved by including predictors such as LRH, DD and UPV using the stepwise regression approach. The inclusion of these variables sequentially increased the R^2 value of the model from 0.771 to 0.864, indicating their combined importance for UCS prediction. The Et prediction model also reached an R2 of 0.884 when incorporating LRH, UPV and DD.

The NLR analysis yielded a highly effective model for predicting UCS, with the best model utilizing four predictors, achieving an R^2 of 0.92 and a minimum RMSE of 7.59. However, the improvement in prediction accuracy compared to MLR was modest. The nonlinear model for predicting Et also showed better performance, with an R^2 of 0.90 and RMSE of 1.12. However, although nonlinear regression could accommodate more complex relationships, the increased complexity did not add significantly to the predictions of the linear model.

The effectiveness of LSTM networks in predicting the mechanical properties of materials, such as UCS and Et, was demonstrated in this study. The analysis of the layers in the LSTM architecture revealed that the model's performance is highly sensitive to the careful configuration of the model. The correlation matrix further supported the presence of input features in explaining the target variables, validating the model's foundation in material property analysis.

By leveraging the power of LSTM networks to learn complex, nonlinear relationships in sequential data, the model achieved remarkable prediction accuracy and high R^2 scores of 0.9844 and 0.9644, as well as low RMSE values for both target variables. The model was reliable, with minimal bias and few outliers. While hyperparameter tuning was conducted through trial and error, a rationale will be provided for the chosen parameters using an optimization method in future work.

Although the results of this work indicate the effectiveness of hybrid regression and LSTM-based models in predicting the mechanical properties of basalt rocks, several limitations must be acknowledged. First, the data set consisted of 134 core samples taken in a selected geological area in Jordan, which may limit the applicability of the models developed to other lithologies or geographical environments. Second, despite considering four non-destructive parameters (Leeb rebound hardness, Schmidt hammer rebound, dry density, and ultrasonic pulse velocity), other factors that might have an impact, such as mineralogical heterogeneity, microcracking, or the level of weathering, were not taken into account. Lastly, the models have been validated in controlled laboratory settings; however, their field-scale applicability, long-term performance, and response to in-situ variability have not been assessed and are to be examined in the future.

CRediT authorship contribution statement

Samer Rababah: Conceptualization, data curation; Formal analysis, Visualization, Writing - original draft; Writing - review & editing.

Mohammad Ali Khasawneh: Conceptualization, Validation, Writing - review & editing.

Hiren Mewada: Conceptualization; Formal analysis, Software, Writing - original draft, Writing - review & editing.

Hussien Aldeeky: Conceptualization; Investigation, Writing - original draft.

Funding

This research received no external funding.

Conflicts of interest

The authors declare no conflicts of interest regarding this manuscript

References

[1] Umrao RK, Singh R, Singh TN. Stability evaluation of hill cut slopes along national highway-13 near Hospet, Karnataka, India. Georisk Assess Manag Risk Eng Syst Geohazards 2015;9:158–70. https://doi.org/10.1080/17499518.2015.1053494.

[2] ISRM (2007) The complete ISRM suggested methods for rock characterization, testing and monitoring. In: Ulusay R, Hudson JA (eds) Suggested methods prepared by the commission on testing methods. International Society for Rock Mechanics, ISRM Turkish Nation n.d.

[3] Heidari M, Khanlari GR, Torabi Kaveh M, Kargarian S. Predicting the Uniaxial Compressive and Tensile Strengths of Gypsum Rock by Point Load Testing. Rock Mech Rock Eng 2012;45:265–73. https://doi.org/10.1007/s00603-011-0196-8.

[4] Fakir M, Ferentinou M, Misra S. An Investigation into the Rock Properties Influencing the Strength in Some Granitoid Rocks of KwaZulu-Natal, South Africa. Geotech Geol Eng 2017;35:1119–40. https://doi.org/10.1007/s10706-017-0168-1.

[5] Umrao RK, Sharma LK, Singh R, Singh TN. Determination of strength and modulus of elasticity of heterogenous sedimentary rocks: An ANFIS predictive technique. Measurement 2018;126:194–201. https://doi.org/10.1016/J.MEASUREMENT.2018.05.064.

[6] Aldeeky H, Al Hattamleh O. Prediction of Engineering Properties of Basalt Rock in Jordan Using Ultrasonic Pulse Velocity Test. Geotech Geol Eng 2018;36:3511–25. https://doi.org/10.1007/s10706-018-0551-6.

[7] Yagiz S. Correlation between slake durability and rock properties for some carbonate rocks. Bull Eng Geol Environ 2011;70:377–83. https://doi.org/10.1007/S10064-010-0317-8/TABLES/4.

[8] Fereidooni D, Karimi Z, Ghasemi F. Non-destructive test-based assessment of uniaxial compressive strength and elasticity modulus of intact carbonate rocks using stacking ensemble models. PLoS One 2024;19:e0302944. https://doi.org/10.1371/JOURNAL.PONE.0302944.

[9] Shahani NM, Zheng X, Liu C, Li P, Hassan FU. Application of soft computing methods to estimate uniaxial compressive strength and elastic modulus of soft sedimentary rocks. Arab J Geosci 2022 155 2022;15:1–19. https://doi.org/10.1007/S12517-022-09671-6.

[10] Malkawi DA, Rabab'ah SR, Sharo AA, Aldeeky H, Al-Souliman GK, Saleh HO. Enhancing of uniaxial compressive strength of travertine rock prediction through machine learning and multivariate analysis. Results Eng 2023;20:101593. https://doi.org/10.1016/J.RINENG.2023.101593.

[11] Barham WS, Rabab'ah SR, Aldeeky HH, Al Hattamleh OH. Mechanical and Physical Based Artificial Neural Network Models for the Prediction of the Unconfined Compressive Strength of Rock. Geotech Geol Eng 2020;38:4779–92. https://doi.org/10.1007/s10706-020-01327-0.

[12] Ling X, Wang M, Yi W, Xia Q, Sun H. Predicting Rock Unconfined Compressive Strength Based on Tunnel Face Boreholes Measurement-While-Drilling Data. KSCE J Civ Eng 2024;28:5946–62. https://doi.org/10.1007/S12205-024-2742-4/METRICS.

[13] Asteris PG, Karoglou M, Skentou AD, Vasconcelos G, He M, Bakolas A, et al. Predicting uniaxial compressive strength of rocks using ANN models: Incorporating porosity, compressional wave velocity, and schmidt hammer data. Ultrasonics 2024;141:107347. https://doi.org/10.1016/J.ULTRAS.2024.107347.

[14] Ghasemi E, Kalhori H, Bagherpour R, Yagiz S. Model tree approach for predicting uniaxial compressive strength and Young's modulus of carbonate rocks. Bull Eng Geol Environ 2018;77:331–43. https://doi.org/10.1007/S10064-016-0931-1/TABLES/7.

[15] Mahmoodzadeh A, Mohammadi M, Ghafoor Salim S, Farid Hama Ali H, Hashim Ibrahim H, Nariman Abdulhamid S, et al. Machine Learning Techniques to Predict Rock Strength Parameters. Rock Mech Rock Eng 2022;55:1721–41. https://doi.org/10.1007/s00603-021-02747-x.

[16] Sabri MS, Jaiswal A, Verma AK, Singh TN. Advanced machine learning approaches for uniaxial compressive strength prediction of Indian rocks using petrographic properties. Multiscale Multidiscip Model Exp Des 2024;7:5265–86. https://doi.org/10.1007/S41939-024-00513-4/FIGURES/18.

[17] Wen T, Li D, Wang Y, Hu M, Tang R. Machine learning methods for predicting the uniaxial compressive strength of the rocks: a comparative study. Front Earth Sci 2024;18:400–11. https://doi.org/10.1007/S11707-024-1101-6/METRICS.

[18] Çanakcı H, Baykasoğlu A, Güllü H. Prediction of compressive and tensile strength of Gaziantep basalts via neural networks and gene expression programming. Neural Comput Appl 2009;18:1031–41. https://doi.org/10.1007/s00521-008-0208-0.

[19] Yagiz S. Assessment of brittleness using rock strength and density with punch penetration test. Tunn Undergr Sp Technol 2009;24:66–74. https://doi.org/10.1016/J.TUST.2008.04.002.

[20] DEHGHAN S, SATTARI G, CHEHREH CHELGANI S, ALIABADI M. Prediction of uniaxial compressive strength and modulus of elasticity for Travertine samples using regression and artificial neural networks. Min Sci Technol 2010;20:41–6. https://doi.org/10.1016/S1674-5264(09)60158-7.

[21] Yagiz S, Karahan H. Prediction of hard rock TBM penetration rate using particle swarm optimization. Int J Rock Mech Min Sci 2011;48:427–33. https://doi.org/10.1016/J.IJRMMS.2011.02.013.

[22] Yagiz S, Sezer EA, Gokceoglu C. Artificial neural networks and nonlinear regression techniques to assess the influence of slake durability cycles on the prediction of uniaxial compressive strength and modulus of elasticity for carbonate rocks. Int J Numer Anal Methods Geomech 2012;36:1636–50. https://doi.org/10.1002/nag.1066.

[23] Beiki M, Majdi A, Dadi Givshad A. Application of genetic programming to predict the uniaxial compressive strength and elastic modulus of carbonate rocks. Int J Rock Mech Min Sci 2013;63:159–69. https://doi.org/10.1016/j.ijrmms.2013.08.004.

[24] Yesiloglu-Gultekin N, Gokceoglu C, Sezer EA. Prediction of uniaxial compressive strength of granitic rocks by various nonlinear tools and comparison of their performances. Int J Rock Mech Min Sci 2013;62:113–22. https://doi.org/10.1016/j.ijrmms.2013.05.005.

[25] Armaghani DJ, Tonnizam Mohamad E, Momeni E, Monjezi M, Sundaram Narayanasamy M. Prediction of the strength and elasticity modulus of granite through an expert artificial neural network. Arab J Geosci 2016;9:48. https://doi.org/10.1007/s12517-015-2057-3.

[26] Singh PK, Tripathy A, Kainthola A, Mahanta B, Singh V, Singh TN. Indirect estimation of compressive and shear strength from simple index tests. Eng Comput 2017;33:1–11. https://doi.org/10.1007/s00366-016-0451-4.

[27] Esmaeili-Falak M, Katebi H, Vadiati M, Adamowski J. Predicting Triaxial Compressive Strength and Young's Modulus of Frozen Sand Using Artificial Intelligence Methods. J Cold Reg Eng 2019;33:04019007. https://doi.org/10.1061/(ASCE)CR.1943-5495.0000188.

[28] Mahdiabadi N, Khanlari G. Prediction of Uniaxial Compressive Strength and Modulus of Elasticity in Calcareous Mudstones Using Neural Networks, Fuzzy Systems, and Regression Analysis. Period Polytech Civ Eng 2019;63:104–14. https://doi.org/10.3311/PPCI.13035.

[29] Teymen A, Mengüç EC. Comparative evaluation of different statistical tools for the prediction of uniaxial compressive strength of rocks. Int J Min Sci Technol 2020;30:785–97. https://doi.org/10.1016/J.IJMST.2020.06.008.

[30] Fang Q, Yazdani Bejarbaneh B, Vatandoust M, Jahed Armaghani D, Ramesh Murlidhar B, Tonnizam Mohamad E. Strength evaluation of granite block samples with different predictive models. Eng Comput 2021;37:891–908. https://doi.org/10.1007/S00366-019-00872-4/FIGURES/14.

[31] Gül E, Ozdemir E, Eren Sarıcı D. Modeling uniaxial compressive strength of some rocks from turkey using soft computing techniques. Measurement 2021;171:108781. https://doi.org/10.1016/j.measurement.2020.108781.

[32] Mahmoodzadeh A, Mohammadi M, Hashim Ibrahim H, Nariman Abdulhamid S, Ghafoor Salim S, Farid Hama Ali H, et al. Artificial intelligence forecasting models of uniaxial compressive strength. Transp Geotech 2021;27:100499. https://doi.org/10.1016/J.TRGEO.2020.100499.

[33] Jin X, Zhao R, Ma Y. Application of a Hybrid Machine Learning Model for the Prediction of Compressive Strength and Elastic Modulus of Rocks. Miner 2022, Vol 12, Page 1506 2022;12:1506. https://doi.org/10.3390/MIN12121506.

[34] Abdi Y, Momeni E, Armaghani DJ. Elastic modulus estimation of weak rock samples using random forest technique. Bull Eng Geol Environ 2023;82:1–20. https://doi.org/10.1007/S10064-023-03154-Y/FIGURES/16.

[35] Benemaran RS, Esmaeili-Falak M. Predicting the Young's modulus of frozen sand using machine learning approaches: State-of-the-art review. Geomech Eng 2023;34:507. https://doi.org/10.12989/GAE.2023.34.5.507.

[36] Taheri-Garavand A, Abdi Y, Momeni E. Smart Estimation of Sandstones Mechanical Properties Based on Thin Section Image Processing Techniques. J Nondestruct Eval 2024;43:1–15. https://doi.org/10.1007/S10921-024-01056-X/TABLES/5.

[37] Chen K, Zhou Y, Dai F. A LSTM-based method for stock returns prediction: A case study of China stock market. Proc - 2015 IEEE Int Conf Big Data, IEEE Big Data 2015 2015:2823–4. https://doi.org/10.1109/BIGDATA.2015.7364089.

[38] Wang J, Li J, Wang X, Wang J, Huang M. Air quality prediction using CT-LSTM. Neural Comput Appl 2021;33:4779–92. https://doi.org/10.1007/S00521-020-05535-W/FIGURES/8.

[39] ISRM. The ISRM Suggested Methods for Rock Characterization, Testing and Monitoring: 2007-2014. Cham, Switzerland: Springer International Publishing; 2015. https://doi.org/10.1007/978-3-319-07713-0.

[40] ASTM D2845. Standard test method for laboratory determination of pulse velocities and ultrasonic elastic constants of rock. ASTM Int 2008:West Conshohocken, PA, USA.

[41] Daniels G, McPhee C, McCurdy P, Sorrentino Y. Non-destructive strength index testing applications for sand failure evaluation. SPE Asia Pacific Oil Gas Conf. Exhib., SPE; 2012, p. SPE-158326.

[42] Corkum AG, Asiri Y, El Naggar H, Kinakin D. The Leeb Hardness Test for Rock: An Updated Methodology and UCS Correlation. Rock Mech Rock Eng 2018;51:665–75. https://doi.org/10.1007/s00603-017-1372-2.

[43] ASTM D5873. Standard Test Methods for Determination of Rock Hardness by Rebound Hammer Method. ASTM Int., West Conshohocken, PA, USA: American Society for Testing and Materials West Conshohocken, PA, USA; 2014.

[44] ASTM D7012. Standard test method for compressive strength and elastic moduli of intact rock core specimens under varying states of stress and temperatures. ASTM Int 2017;10:West Conshohocken, PA, USA.

[45] Bejarbaneh BY, Bejarbaneh EY, Amin MFM, Fahimifar A, Jahed Armaghani D, Majid MZA. Intelligent modelling of sandstone deformation behaviour using fuzzy logic and neural network systems. Bull Eng Geol Environ 2018;77:345–61. https://doi.org/10.1007/S10064-016-0983-2/TABLES/11.

[46] Aldeeky H, Al Hattamleh O, Rababah S. Assessing the uniaxial compressive strength and tangent Young's modulus of basalt rock using the Leeb rebound hardness test. Mater Construcción 2020;70:230. https://doi.org/10.3989/mc.2020.15119.

[47] Aladejare AE, Alofe ED, Onifade M, Lawal AI, Ozoji TM, Zhang Z-X. Empirical Estimation of Uniaxial Compressive Strength of Rock: Database of Simple, Multiple, and Artificial Intelligence-Based Regressions. Geotech Geol Eng 2021;39:4427–55. https://doi.org/10.1007/s10706-021-01772-5.

[48] EN ISO 14689. Geotechnical investigation and testing. Identification, description and classification of rock 2018. https://doi.org/10.3403/BSENISO14689.

[49] Deere D V, Miller RP. Engineering classification and index properties for intact rock 1966.

[50] Kochukrishnan S, Krishnamurthy P, D Y, Kaliappan N. Comprehensive study on the Python-based regression machine learning models for prediction of uniaxial compressive strength using multiple parameters in Charnockite rocks. Sci Reports 2024 141 2024;14:1–12. https://doi.org/10.1038/s41598-024-58001-1.

[51] Tang Z, Li S, Huang S, Huang F, Wan F. Indirect Estimation of Rock Uniaxial Compressive Strength from Simple Index Tests: Review and Improved Least Squares Regression Tree Predictive Model. Geotech Geol Eng 2021;39:3843–62. https://doi.org/10.1007/S10706-021-01731-0/FIGURES/2.

[52] Li C, Zhou J, Dias D, Du K, Khandelwal M. Comparative Evaluation of Empirical Approaches and Artificial Intelligence Techniques for Predicting Uniaxial Compressive Strength of Rock. Geosci 2023, Vol 13, Page 294 2023;13:294. https://doi.org/10.3390/GEOSCIENCES13100294.

[53] Esmaeili-Falak M, Benemaran RS. Ensemble Extreme Gradient Boosting based models to predict the bearing capacity of micropile group. Appl Ocean Res 2024;151:104149. https://doi.org/10.1016/J.APOR.2024.104149.

[54] Zhu Y, Huang L, Zhang Z, Bayrami B. Estimation of splitting tensile strength of modified recycled aggregate concrete using hybrid algorithms. Steel Compos Struct 2022;44:389. https://doi.org/10.12989/SCS.2022.44.3.389.

[55] Kou H, Quan J, Guo S, Hassankhani E. Light and normal weight concretes shear strength estimation using tree-based tunned frameworks. Constr Build Mater 2024;452:138955. https://doi.org/10.1016/J.CONBUILDMAT.2024.138955.

[56] Yaychi BM, Esmaeili-Falak M. Estimating Axial Bearing Capacity of Driven Piles Using Tuned Random Forest Frameworks. Geotech Geol Eng 2024;42:7813–34. https://doi.org/10.1007/S10706-024-02952-9/FIGURES/8.

[57] Esmaeili-Falak M, Sarkhani Benemaran R. Application of optimization-based regression analysis for evaluation of frost durability of recycled aggregate concrete. Struct Concr 2024;25:716–37. https://doi.org/10.1002/SUCO.202300566;WGROUP:STRING:PUBLICATION.